Research Article

P-body formation is required for yeast proliferation in the phyllosphere

Fuka Sekioka[1], Kosuke Shiraishi[1*], Miho Akagi[1], Akari Habata[1], Yumi Arima[1], Yasuyoshi Sakai[2,3] & Hiroya Yurimoto[1]

[1] Division of Applied Life Sciences, Graduate School of Agriculture, Kyoto University, Kitashirakawa-Oiwake, Sakyo-ku, Kyoto 606-8502, Japan

[2] Graduate School of Advanced Integrated Studies in Human Survivability, Kyoto University, Kitashirakawa-Oiwake, Sakyo-ku, Kyoto 606-8306, Japan

[3] Department of Bioscience and Biotechnology, Faculty of Bioenvironmental Sciences, Kyoto University of Advanced Science, Kameoka, Kyoto 621-8555, Japan

[*]Correspondence

Kosuke Shiraishi, Ph.D.

Division of Applied Life Sciences, Graduate School of Agriculture, Kyoto University, Kitashirakawa-Oiwake, Sakyo-ku, Kyoto 606-8502, Japan

Phone: +81-75-753-6387

Fax: +81-75-753-6454

E-mail: shiraishi.kosuke.7t@kyoto-u.ac.jp

Abstract

Processing bodies (P-bodies) are major cytosolic ribonucleoprotein granules involved in post-transcriptional regulation. Yeast has been an invaluable model for elucidating the functions of P-bodies under laboratory conditions. However, the physiological significance of P-bodies in natural environments remains unclear. Here, we demonstrate that P-body formation is required for yeast proliferation in the phyllosphere, the aerial parts of plants. Deletion of *EDC3*, a gene critical for P-body formation, impaired proliferation of the methanol-utilizing yeast *Candida boidinii* on *Arabidopsis thaliana* leaves where the yeast assimilates methanol as the carbon source while adapting to changes in environmental conditions. *In vitro* experiments showed that P-bodies contribute to the spatiotemporal regulation of methanol-induced mRNAs (mimRNAs). These mimRNAs form cytosolic dot structures (termed mimRNA granules) that harbor multiple kinds of mimRNAs. In the *edc3Δ* strain, the formation of mimRNA granules was reduced along with a decrease in mimRNA abundance. Under oxidative stress, colocalization of P-bodies with mimRNA granules markedly increased and growth of the *edc3Δ* strain on methanol was suppressed, suggesting active sequestration of mimRNAs within P-bodies as a stress tolerance response. Time-lapse microscopy revealed dynamic interactions between P-bodies and mimRNAs granules with transient colocalization. Together, our findings indicate that P-bodies function as temporal storage sites where mimRNAs are protected from degradation in the phyllosphere.

Introduction

Ribonucleoprotein (RNP) granules are membrane-less organelles formed through liquid–liquid phase separation (LLPS), concentrating RNAs and RNA-binding proteins into condensates within the cytosol or nucleus (Ripin & Parker, 2023). Among these, processing bodies (P-bodies) are recognized as major cytosolic RNP granules that function as hubs for post-transcriptional regulation, particularly under stress conditions (Decker & Parker, 2012; Kedersha & Anderson, 2009). P-bodies contain RNA-binding proteins and translationally repressed mRNAs, mediating mRNA storage and translational repression (Nissan et al., 2010). These granules are highly dynamic, undergo rapid and reversible assembly and disassembly, and frequently exchange components with other RNP granules (Buchan, 2024; Decker & Parker, 2012), including stress granules (SGs), which harbor translation initiation complexes (Swisher & Parker, 2010). P-bodies and SGs allow cells to protect key mRNAs from degradation and modulate their availability for translation in response to environmental stimuli through transient mRNA sequestration, offering an energy-efficient strategy compared to continuous cycles of mRNA degradation and *de novo* synthesis. Yeast has been an invaluable model for elucidating the functions of RNP granules under controlled laboratory conditions. Yet, the physiological relevance of RNP granules in complex and changing natural environments remains largely unexplored.

The phyllosphere, the aerial parts of plants, is one of the largest microbial habitats in nature (Ruinen, 1956). The total surface area of both sides of leaves on Earth is estimated at 6.4×10^8 km^2 and harbors a wide array of microbes, including yeasts (Morris & Kinkel, 2002). Despite its ecological richness, the phyllosphere represents a harsh environment characterized by oxidative stress, elevated temperatures and nutrient limitations (Beattie & Lindow, 1995; Lindow & Brandl, 2003; Vorholt, 2012). To survive under these conditions, phyllosphere microbes have evolved diverse adaptive mechanisms, including robust stress responses and metabolic flexibility.

Among these microbial residents, methylotrophic microbes have developed unique strategies to adapt to the phyllosphere environment. A key adaptation is their ability to utilize methanol, which is released as a product of pectin demethylesterification in plant cell walls during growth and is available for microbial use as a carbon source (Fall & Benson, 1996; Nemecek-Marshall et al., 1995; Yurimoto et al., 2021). Our previous study demonstrated that methanol concentrations on leaf surfaces oscillate diurnally, rising during the dark period (0.048–0.21%) and falling during the light period (0.014–0.015%) on growing plant leaves, while remaining elevated (≥0.8%) on wilting or dead plant leaves (Kawaguchi et al., 2011). Using the methylotrophic yeast *Candida boidinii*, which

is frequently isolated from plant samples (Cadete et al., 2012; Mota et al., 2024), we showed that the yeast proliferates by using methanol as the carbon source on plant leaves and adapts to oscillating methanol availability by adjusting the transcription of methanol-induced genes in response to local methanol concentrations (Kawaguchi et al., 2011). Building on these findings, and drawing on recent findings that mRNAs encoding metabolic enzymes can be sequestered in P-bodies for temporal storage prior to translation (Lavut & Raveh, 2012; Lui et al., 2014; Standart & Weil, 2018), we hypothesized that *C. boidinii* adapts to environmental methanol availability not only transcriptionally, but also post-transcriptionally via P-body–mediated mRNA regulation.

Yeast methylotrophy involves various enzymes localized in either peroxisomes or the cytosol (Yurimoto et al., 2011) (cf. Figure2-figure supplement 1). In peroxisomes, alcohol oxidase (AOD) and dihydroxyacetone synthase (DAS) catalyze methanol oxidation and formaldehyde fixation, while catalase (CTA) and peroxisomal peroxidase (PMP20) detoxify reactive oxygen species (ROS). In the cytosol, formaldehyde dehydrogenase (FLD), *S*-formylglutathione hydrolase (FGH) and formate dehydrogenase (FDH) further metabolize formaldehyde and formate to CO_2, yielding energy. Transcription of these enzymes is strongly induced by methanol, resulting in the accumulation of large quantities of methanol-induced mRNAs (mimRNAs) prior to protein synthesis. However, the intracellular fates of these mRNAs—whether they are stored, degraded or relocalized—remain unknown.

In this study, we investigated whether P-bodies contribute to yeast survival in the phyllosphere using a nature-mimicking experimental system with the methylotrophic yeast *C. boidinii* and plant *Arabidopsis thaliana*. We also examined how yeast P-bodies regulate the intracellular dynamics of mimRNAs to support metabolic adaptation under methanol growth conditions. Our findings provide new insight into the role of P-bodies in natural environments by highlighting their importance in the spatiotemporal regulation of mimRNAs that promote microbial adaptation in the phyllosphere.

Results

P-body formation is required for yeast proliferation in the phyllosphere

We first examined whether *C. boidinii* forms P-bodies in the phyllosphere using Edc3-Venus as a fluorescent marker because Edc3 localizes to P-bodies and is essential for their formation (Decker et al., 2007; Tishinov & Spang, 2021). The wild-type (WT) strain expressing Edc3-Venus (strain Edc3-V) was inoculated onto growing leaves of *A. thaliana* (2–3 weeks post-germination). Yeast cells were collected over time from plants grown under a daily light/dark cycle. Fluorescence microscopy detected cytosolic dots in yeast cells at 1, 3 and 7 days post-inoculation (Figure 1A). Quantitative analysis showed that the dot formation of Edc3-Venus was similar under light and dark conditions and that the number of dots slightly increased over time (Figure 1B), demonstrating the constitutive presence of P-bodies in *C. boidinii* on leaves.

To assess the physiological significance of P-body formation in the phyllosphere, we disrupted the *EDC3* gene. The WT and *edc3Δ* strains expressing Venus fused to Dcp2, another P-body marker (Buchan et al., 2008), were examined under both laboratory and phyllosphere conditions. In both synthetic methanol (SM) medium (Figure 1C, D) and on *A. thaliana* leaves (Figure 1E, F), deletion of *EDC3* led to a marked reduction in Dcp2-Venus dots, confirming the importance of Edc3 in P-body formation in *C. boidinii*. Next, we investigated whether P-body formation influences yeast proliferation in the phyllosphere. The WT and *edc3Δ* strains expressing Venus under the constitutive *ACT1* promoter were inoculated onto growing leaves and monitored for seven days. In the WT strain, confocal microscopy showed progressive proliferation of fluorescent cells (Figure 1G), which was consistent with an approximately 4-fold increase in cell number as measured by flow cytometry (FCM) (Figure 1H). In contrast, no significant increase in cell number was observed in the *edc3Δ* strain (Figure 1G, H), indicating that P-body formation is required for yeast proliferation on plant leaves.

Because the phyllosphere environment changes over the course of plant development (Kawaguchi et al., 2011; Shiraishi et al., 2015), we examined P-body formation in *C. boidinii* at different stages of plant growth: growing (2–3 weeks), matured (5–6 weeks), wilting (2 months) and dead (3 months post-germination). Edc3-Venus dots were consistently observed in yeast cells collected across all plant stages (Figure 1–figure supplement 1A). We further asked whether SGs form under these conditions using the *C. boidinii* WT strain expressing Pbp1-Venus, a marker for SGs (Shiraishi et al., 2018) (strain Pbp1-V). No cytosolic dots were detected in strain Pbp1-V on any leaf of any growth stage under the tested conditions (Figure 1–figure supplement 1B). These observations demonstrate that only P-bodies and not SGs are formed in *C. boidinii* on leaf

surfaces.

P-bodies partially but continuously colocalize with "methanol-induced mRNA granules (mimRNA granules)"

We hypothesized that P-bodies contribute to the post-transcriptional regulation of genes encoding enzymes for methanol metabolism (shown in Figure 2–figure supplement 1), supporting yeast proliferation on leaves. To test this physiological role of P-bodies in the phyllosphere, we investigated the intracellular dynamics of P-bodies and mimRNAs. *DAS1* mRNA (as a representative mimRNA) was visualized by a Venus-tagged U1A-based RNA system (Takizawa & Vale, 2000) (see Figure 2–figure supplement 2A for methodological overview) and P-bodies by Cerulean-tagged Edc3 in the WT strain (strain Edc3-C/DAS1m-V). Validity of the U1A system in *C. boidinii* was confirmed by colocalization between U1A-based signals and fluorescence *in situ* hybridization (FISH) (Long et al., 1995) signals for *DAS1* mRNA (Figure 2–figure supplement 2B, C), as well as a complementary growth assay (Figure 2–figure supplement 2D). Strain Edc3-C/DAS1m-V was then inoculated onto growing *Arabidopsis* leaves and confocal microscopy was used to detect cytosolic dots of both Edc3-Cerulean and Venus-tagged *DAS1* mRNA, some of which colocalized with each other (Figure 2A). Fluorescence microscopy of yeast cells collected from leaves provided clearer images and confirmed dot formation under both light and dark conditions, with approximately 5% of their fluorescent signals colocalizing (Figure 2B, C). Similar patterns were detected in yeast cells on wilting leaves (Figure 2–figure supplement 3A, B).

Since this is the first time that mimRNAs have been observed to form cytosolic dots, we next conducted *in vitro* experiments to test whether Edc3-Cerulean and Venus-tagged *DAS1* mRNA dots are distinct. Strain Edc3-C/DAS1m-V grown on synthetic glucose (SD) medium was transferred to SM medium to induce the expression of genes involved in methanol metabolism. Time-course microscopy showed that Edc3-Cerulean dots were present throughout, with moderate changes in number (0.3 ~ 1.7 dots per cell) (Figure 2D, E). By contrast, Venus-tagged *DAS1* mRNA dots appeared only under methanol growth conditions. The dot number increased sharply at 2 h and remained at a comparable level with modest variations until 8 h (3.5 ~ 5.9 dots per cell) (Figure 2D, E). During this period, approximately 30% of Edc3-Cerulean dots colocalized with Venus-tagged *DAS1* mRNA dots (Figure 2E). These results indicate that Venus-tagged *DAS1* mRNA dots and Edc3-Cerulean dots are distinct structures, although a subset of these structures colocalizes with each other during growth on methanol.

To characterize the mimRNA dots further, we visualized six additional mimRNAs: *AOD1*, *FLD1*, *FGH1*, *FDH1*, *PMP20* and *CTA1* (cf. Figure 2–figure supplement 1). We confirmed the functionality of the U1A system for mimRNAs encoding cytosolic enzymes by a complementary growth assay, using *FLD1* mRNA (Figure 2–figure supplement 2D). Fluorescence microscopy showed dot formation for all tested mimRNAs under methanol growth conditions, although dot numbers varied (Figure 2F, G). To assess the intracellular dynamics of multiple mimRNAs, we employed the MS2-based RNA system, another method for visualizing mRNAs (Bertrand et al., 1998b). Approximately 40% of *DAS1* mRNA dots visualized by the MS2 system overlapped with those detected by the U1A system in strain DD during growth on methanol (Figure 2H, I). We then visualized *AOD1* mRNA or *FLD1* mRNA with the Venus-tagged U1A-based system in strains expressing Cerulean-tagged *DAS1* mRNA by the MS2 system (strain AD and strain FD, respectively). In both strains, partial colocalization was observed (Figure 2H), with a comparable rate to strain DD (Figure 2I), suggesting that multiple mimRNAs share granules at least in part. Together, we defined methanol-induced cytosolic dots enriched with multiple mimRNAs as "mimRNA granules".

P-bodies contribute to the post-transcriptional regulation of mimRNAs

To further investigate the role of P-bodies in the post-transcriptional regulation of mimRNAs, we compared *DAS1* mRNA dot formation in the WT and *edc3Δ* strains (strain DAS1m-V and strain edc3Δ-DAS1m-V, respectively). Fluorescence microscopy detected Venus-tagged *DAS1* mRNA dots in both strains during growth on methanol (Figure 3A). However, quantitative analysis revealed significantly fewer dots in strain edc3Δ-DAS1m-V compared to strain DAS1m-V (Figure 3B), suggesting that P-bodies contribute to the formation of mimRNA granules. To assess the impact of P-bodies on transcript abundance, we measured the *DAS1* transcript level by qRT-PCR. *DAS1* transcript levels were lower in the *edc3Δ* strain than in the WT (Figure 3C). Similar results were obtained for *AOD1* mRNA (Figure 3–figure supplement 1A). These results in conjunction with previous suggestions (Wang et al., 2018) led us to infer that P-bodies serve as storage sites for mimRNAs and protect them from degradation by sequestration. Protein levels of DAS and AOD (Figure 3–figure supplement 1B, C) and cell growth on SM medium (Figure 3–figure supplement 1D) in the *edc3Δ* strain were comparable to those of the WT strain under the tested conditions.

The phyllosphere is a harsh environment where yeast cells experience various stresses, including oxidative stress and elevated temperatures, many of which are known to enhance P-body formation (Teixeira & Parker, 2007). This prompted us to speculate

that P-bodies sequester mimRNAs more actively under these stress conditions to enhance the post-transcriptional regulation of mimRNAs and improve yeast survival on plant surfaces. To test this, we first examined P-body formation in *C. boidinii* exposed to various stresses. Treatment with 5 mM H_2O_2 (oxidative stress), 37°C (heat shock) or 3 M NaCl (salt stress) increased both the number of Edc3-Venus dots and proportion of cells containing at least one dot, indicating enhanced P-body formation (Figure 3D). The strongest effect was observed under oxidative stress, with an average of 1.69 dots per cell and 95.6% cells containing at least one dot.

Subsequently, we examined the intracellular dynamics of P-bodies and mimRNAs under oxidative stress during growth on methanol. Strain Edc3-C/DAS1m-V was exposed to 5 mM H_2O_2 for 1 hour and analyzed by fluorescence microscopy. Following oxidative stress, the colocalization rate of Edc3-Cerulean dots with Venus-tagged *DAS1* mRNA dots increased from approximately 30% to 60% (Figure 3E, F), indicating that P-bodies actively sequester mimRNAs. Heat shock evoked similar increases, while salt stress did not result in a significant change (Figure 3–figure supplement 2A, B). We also monitored the intracellular dynamics of P-bodies and mimRNAs during recovery from oxidative stress. Strain Edc3-C/DAS1m-V, after being exposed to 5 mM H_2O_2 for 1 hour, was transferred to SM medium and observed after 1 hour. The colocalization rate declined from approximately 60% to 40%, suggesting that P-bodies release mimRNAs back into the cytosol (Figure 3E, F).

We next evaluated the role of P-bodies in yeast survival under oxidative stress. Deletion of *EDC3* markedly reduced P-body formation, as indicated by fewer dot number of Dcp2-Venus (Figure 3G, H), and decreased *DAS1* transcript levels (Figure 3I). These results were consistent with our observations under normal conditions (cf. Figure 1C, D, 3C). We then performed a spot assay using SM agar plates with or without H_2O_2. Growth of the *edc3Δ* strain was impaired under oxidative stress, whereas no clear difference was observed under normal conditions (Figure 3J). The expression of Edc3-Venus restored stress tolerance. These results suggest that sequestration of mimRNAs into P-bodies enhances yeast tolerance to oxidative stress, likely by protecting mimRNAs from stress-induced degradation.

mimRNA granule formation is conserved among methylotrophic yeasts and is regulated in accordance with the transcript levels

We next investigated how mimRNA granule formation is regulated. Fluorescence microscopy showed that Venus fluorescence in strain DAS1m-V remained localized to the DAPI-stained nucleus until 2–2.5 h after the medium shift, whereas cytosolic dot

structures began to appear around 2 h after the shift (Figure 4A, B). Quantitative analysis showed that the number of Venus-tagged *DAS1* mRNA dots started to increase at 2 h, peaked for the next 1 to 2 hours, and then declined moderately (Figure 4C). A similar mountain-shaped curve pattern was observed at the *DAS1* transcript level (Figure 4D). DAS protein levels began to increase at 2.5 h (Figure 4E), 0.5 h after the rise in both Venus-tagged *DAS1* mRNA dot number and *DAS1* mRNA level. Similar patterns were obtained for the other tested mimRNAs (Figure 4–figure supplement 1A-M), suggesting that mimRNA granule formation is induced by methanol and is regulated in accordance with the transcript levels of methanol-induced genes. To further test the correlation between granule formation and transcript levels of mimRNAs, strain DAS1m-V grown on SD medium was transferred to SM medium supplemented with either 0.005% methanol (low-methanol) or 0.5% methanol (high-methanol), and harvested 3 h after the medium shift for microscopy and qRT-PCR analyses. Under low-methanol conditions, both the number of Venus-tagged *DAS1* mRNA dots and *DAS1* transcript levels were lower than those observed under high-methanol conditions (Figure 4–figure supplement 2A-C), supporting our idea that mimRNA granule formation correlates with its transcript level. In addition to *C. boidinii*, we observed dot structures of methanol-induced *AOX1* mRNA in *Komagataella phaffii*, another methylotrophic yeast, following a medium shift from SD to SM (Figure 4–figure supplement 3). This finding suggests that the regulatory mechanism of mimRNA granule formation is conserved among methylotrophic yeasts.

To compare the regulation of dot formation between mimRNAs and non-methanol-induced mRNAs, we visualized *TDH3*, *ADH1* and *ACT1* mRNAs in *C. boidinii* using the U1A system. These mRNAs encode the glycolytic enzyme glyceraldehyde-3-phosphate dehydrogenase (GAPDH), alcohol dehydrogenase involved in ethanol assimilation, and actin, respectively (Sasano et al., 2008; Wylin et al., 1998; Yurimoto et al., 2004). In contrast to *DAS1* mRNA (which showed a dramatic increase in dot formation under methanol growth conditions), Venus-tagged *TDH3* and *ADH1* mRNAs formed dots under all tested conditions. *ACT1* mRNA exhibited only a few dots during growth on methanol and ethanol (Figure 4F-J). Because *TDH3* mRNA formed dots under all tested conditions, we examined its dot formation during methanol induction. Unlike *DAS1* mRNA, Venus-tagged *TDH3* mRNA formed cytosolic dots even before methanol induction (Figure 4–figure supplement 4A), and the number of dots decreased after the medium shift to SM medium (Figure 4–figure supplement 4B). The *TDH3* transcript levels decreased after the medium shift (Figure 4–figure supplement 4C) and GAPDH protein was detected under all conditions (Figure 4–figure supplement 4D),

suggesting that *TDH3* mRNA dots are not induced by methanol. We also examined colocalization of Edc3-Cerulean with Venus-tagged *TDH3* mRNA dots during growth on methanol using strain Edc3-C/TDH3m-V. Under normal conditions, the colocalization rate was approximately 7%, which increased to 15% after 1 h of oxidative stress treatment (Figure 4–figure supplement 5A, B).

Spatiotemporal properties and dynamics of mimRNA granules

Finally, we sought to characterize the properties of mimRNA granules. To this end, we examined their dynamics alongside P-bodies in live cells during cultivation on methanol. Time-lapse microscopy revealed that *DAS1* mRNA dots were dynamic in undergoing rapid assembly and disassembly, similar to P-bodies (Figure 5A, Figure 5—video 1). For example, a new Venus-tagged *DAS1* mRNA dot appeared at 56 seconds in the video, which colocalized with an Edc3-Cerulean dot from 1 min 24 s to 2 min 48 s, and disappeared at 3 min 16 s, while the Edc3-Cerulean dots remained. These observations indicate that P-bodies and mimRNA granules dynamically interact with each other. Additionally, at 7 min 56 s, a Venus-tagged *DAS1* mRNA dot appeared without colocalizing with a P-body; this granule remained at the same site at 8 min 24 s but disappeared at 8 min 52 s, suggesting possible relocalization of the mimRNA.

To investigate how mimRNAs associated with P-bodies respond to translational regulation, we treated strain Edc3-C/DAS1m-V with puromycin (PMC) and cycloheximide (CHX) (Riggs et al., 2020). PMC promotes the accumulation of ribosome-free mRNAs (Cougot et al., 2004; Zheng et al., 2008), thereby promoting RNP granule formation, including P-bodies (Eulalio et al., 2007; Kedersha et al., 2005). Consistent with previous studies, PMC treatment increased the number of Edc3-Cerulean dots. We also observed that their colocalization with Venus-tagged *DAS1* mRNA dots increased without significantly altering the total number of *DAS1* mRNA dots (Figure 5B, C). CHX is known to stall ribosomes on mRNAs, which prevents the accumulation of ribosome-free mRNAs (Schneider-Poetsch et al., 2010) and inhibits the formation of RNP granules, including P-bodies (Andrei et al., 2005; Grousl et al., 2009; Kedersha et al., 2000). As expected, CHX suppressed Edc3-Cerulean dot formation and reduced colocalization with Venus-tagged *DAS1* mRNA dots, while partially reducing the number of *DAS1* mRNA dots (Figure 5B, C).

In addition, we treated strain Edc3-C/DAS1m-V with 1,6-hexanediol (HXD), which disrupts LLPS-mediated granules (Kroschwald et al., 2015). Similar to CHX, HXD treatment inhibited the formation of Edc3-Cerulean dots and partially reduced the number of Venus-tagged *DAS1* mRNA dots (Figure 5D, E). These results suggest that

some mimRNA granules are resistant to HXD, while P-bodies are significantly suppressed, further indicating that mimRNAs can also accumulate at P-body-independent sites. Therefore, we explored potential locations of mimRNAs other than P-bodies. The endoplasmic reticulum (ER) and peroxisomes were visualized using mCherry-tagged localization sequences (Gould et al., 1989; Lajoie et al., 2012) and actin patches (Amberg, 1998) were stained with rhodamine-phalloidin. Venus-tagged *DAS1* mRNA dots were also detected in association with these compartments (Figure 5–figure supplement 1A-D), raising the possibility of an additional layer of spatial regulation linked to the metabolic state and environmental conditions.

Discussion

We demonstrate that P-body formation is required for the proliferation of methylotrophic yeast *C. boidinii* in the phyllosphere where the yeast uses methanol as the carbon source while adapting to the varying environmental conditions. In the leaf environment, P-bodies play key roles in post-transcriptional regulation of methanol-induced genes. Methanol triggers the transcription of genes involved in methanol assimilation, leading to the accumulation of mimRNAs in the cytosol. These mimRNAs form cytosolic "mimRNA granules", likely containing both ribosome-free and ribosome-associated transcripts, which dynamically interact with P-bodies. Under stresses such as oxidative stress, P-bodies actively sequester mimRNAs to protect them from degradation and release them into the cytosol upon stress removal, potentially for translation. This dynamic interaction enables *C. boidinii* to modulate mimRNAs post-transcriptionally, supporting its adaptation to changing leaf environments (Figure 6).

Here, we demonstrate the significance of yeast P-bodies in a natural environment, specifically the phyllosphere. Our observation that mimRNAs are sequestered by P-bodies on *Arabidopsis* leaves (Figure 2A–C and Figure 2–figure supplement 3), together with *in vitro* results, including their dynamic properties during transient colocalization (Figure 5A, Figure 5–video 1), supports the following model: P-bodies serve as storage sites for mimRNAs, recruiting these transcripts for protection from degradation and releasing them into the cytosol for translation in response to environmental cues. This mechanism likely promotes energy conservation by preserving critical transcripts and minimizing the need for constant mRNA synthesis. This interpretation aligns with previous reports showing that highly expressed mRNAs are often sequestered in P-bodies (Lavut & Raveh, 2012) and that stored mRNAs can re-enter the translational pool when conditions change (Bhattacharyya et al., 2006; Brengues et al., 2005; Parker & Sheth, 2007).

We examined mimRNA granule formation and their colocalization with P-bodies on *Arabidopsis* leaves under light and dark conditions. Although methanol concentrations are higher during the dark period (Kawaguchi et al., 2011), both the number of mimRNA granules (1.2–1.4 dots per cell) and their colocalization rate with P-bodies (~5%) remained low and largely unchanged between light and dark conditions (Figure 2C). Similar results were obtained from cells observed on wilting leaves (Figure 2–figure supplement 3), despite their elevated methanol levels (Kawaguchi et al., 2011). This contrasts with *in vitro* assays (Figure 4–figure supplement 2) where mimRNA granule formation clearly increased with higher methanol concentrations, i.e., 0.5% versus 0.005%. These findings suggest that granule formation does not depend solely on

methanol in the phyllosphere, but is influenced by additional environmental factors, such as stress-specific signaling. Additionally, mimRNAs may be rapidly directed to translation, limiting their accumulation into granules or P-bodies to survive under nutrient-scarce conditions.

The spatiotemporal regulation of mimRNAs appeared to be especially critical under stress conditions, notably oxidative stress (Figure 3). In the phyllosphere, microbial cells are exposed to ROS generated by photosynthesis and to sunlight, which can damage nucleic acids and other cellular components. Microbes deploy protective mechanisms such as pigment production (Jacobs et al., 2005) and DNA repair (Gunasekera & Sundin, 2006) for survival. Our findings suggest that sequestration of mimRNAs into P-bodies represents an additional protective strategy, shielding these transcripts from ROS-induced degradation.

It is possible that P-bodies selectively sequester mimRNAs over non-methanol-induced mRNAs under stress during growth on methanol: ~60% of P-bodies were associated with mimRNAs under oxidative stress, compared to only 15% with *TDH3* non-methanol-induced mRNAs (Figure 3E, F, Figure 4–figure supplement 5). This suggests that P-bodies prioritize the storage of mimRNAs during stress, while non-essential mRNAs are more likely targeted for degradation and recycling. Our interpretation is supported by previous studies showing that P-bodies regulate translation selectively to optimize cell survival (Jang et al., 2019; Sorenson & Bailey-Serres, 2014). However, the molecular mechanisms governing the selective sequestration of mimRNAs in methylotrophic yeasts under methanol growth conditions remain to be elucidated. The principle of selectivity in cellular regulation extends beyond RNA. Our previous study showed that peroxisomes undergo selective autophagy, i.e., pexophagy (Oku & Sakai, 2016) in *C. boidinii* on the leaf surface in response to light/dark cycles, while non-selective bulk autophagy, i.e., macroautophagy occurs continuously (Kawaguchi et al., 2011). Similarly, the yeast nitrate reductase Ynr1 escapes degradation via a selective autophagy termed the cytoplasm-to-vacuole targeting (CVT) pathway (Hutchins & Klionsky, 2001; Scott et al., 1997) on growing leaves but becomes targeted on aged leaves (Shiraishi et al., 2015). Together, these studies illustrate a microbial strategy: the selective preservation and deployment of cellular components in response to environmental changes and nutrient availability.

While our results highlight the importance of P-bodies in mimRNA sequestration, we do not exclude their broader roles in supporting yeast proliferation in the phyllosphere. Since P-bodies influence the quality and fate of various transcripts (Wang et al., 2018),

they may also sequester other mRNAs essential for yeast proliferation, including those involved in autophagy (Kawaguchi et al., 2011). Beyond RNA regulation, P-bodies can safeguard a key kinase protein under low nutrient conditions, protecting it from degradation and enabling proper stress responses (Zhang et al., 2018). Similar protective roles may apply to other essential proteins in the phyllosphere. Furthermore, yeast P-bodies interact with other RNP granules, such as hybrid granules induced by hypoosmotic stress and SGs (Escalante & Gasch, 2021), suggesting that loss of P-body formation could disrupt important inter-granule communication. Taken together, while mimRNA sequestration is a key function, P-bodies are likely to support yeast adaptation to the phyllosphere through multiple mechanisms: regulating mRNA turnover beyond mimRNAs, stabilizing key proteins and engaging in dynamic interactions with other RNP granules to meet the challenges of complex plant-surface environments.

In addition to P-bodies, mimRNA accumulation was observed at membrane-bound organelles such as the ER and peroxisomes (Figure 5–figure supplement 1). The localization of mRNAs to these compartments is increasingly recognized as a key layer of spatial control for translation (Dahan et al., 2022; Morales-Polanco et al., 2021; Pilaz et al., 2023; Singer-Krüger & Jansen, 2014). Various mRNAs have been reported to be targeted to the ER for co-translational processing (Aronov et al., 2007; Fundakowski et al., 2012; Reid & Nicchitta, 2015). A recent study showed that up to 80% of *PEX* mRNAs that encode peroxins essential for the formation and function of peroxisomes are translated locally at peroxisomes (Dahan et al., 2022; Zipor et al., 2009). Notably, only about 30% of *DAS1* mRNA localized to peroxisomes (Figure 5–figure supplement 1), suggesting that mimRNAs such as *DAS1* and *AOD1* are primarily translated at the ER, with their protein products subsequently transported to peroxisomes via peroxisomal targeting sequences (PTS) (Gould et al., 1989). This difference may reflect the temporal distinction in protein demand —peroxins are needed for peroxisome biogenesis whereas methanol-metabolizing enzymes like DAS function after peroxisomes are formed.

Another key feature of mimRNA regulation we observed is their ribosome-free state when sequestered in P-bodies, consistent with previous studies. Treatment with PMC, which generates ribosome-free mRNAs, enhanced P-body formation and mimRNA colocalization, whereas CHX, which stalls ribosomes on mRNAs, suppressed both (Figure 5B, C). These results further support previous reports (Cougot et al., 2004; Zheng et al., 2008) showing that translationally inactive, ribosome-free mRNAs accumulate in P-bodies.

In conclusion, our study demonstrates that P-bodies are required for yeast

proliferation in the phyllosphere. They function as hubs for the temporary storage of mimRNAs, enabling yeast cells to respond rapidly to the complex and changing phyllosphere environment. These findings advance our understanding of post-transcriptional regulation and RNP granule biology in natural microbial ecosystems, while also opening new avenues for investigating eukaryotic microbial dynamics.

1 **Materials and methods**

2 **Appendix 1-Key resources table**

Reagent type (species) or resource	Designation	Source or reference	Identifiers	Additional information
Gene	*C. boidinii genome*	(Tani et al., 1985)		*Candia boidinii* strain AOU-1
Gene	*K. phaffii genome*	(Sakai et al., 1998)		*Komagataella phaffii* strain PPY12
Gene	*CbDCP2*	This study		Registered at the DDBJ/EMBL/GenBank under accession number LC889013.
Gene	*CbKAR2*	This study		Registered at the DDBJ/EMBL/GenBank under accession number LC889015.
Gene	*CERULEAN*	This study		Encoding fluorescent protein Cerulean, codon-optimized for *C. boidinii*; registered in DDBJ/EMBL/GenBank (Accession No. LC889016)
Gene	BSD^r	This study		Encoding blasticidin *S* deaminase, codon-optimized for *C. boidinii*; registered in DDBJ/EMBL/GenBank (Accession No. LC889017)

Gene	*U1A*	This study		Encoding U1 small nuclear ribonucleoprotein A (U1A), codon-optimized for *C. boidinii*; registered in DDBJ/EMBL/GenBank (Accession No. LC889018)
Gene	*MS2*	This study		Encoding MS2 coat protein, codon-optimized for *C. boidinii*; registered in DDBJ/EMBL/GenBank (Accession No. LC889019)
Gene	*4 x U1A binding sequence (4xU1Abs)*	(Takizawa & Vale, 2000)		Amplified by PCR from the plasmidpSYN5908-1 purchased from TaKaRa Bio. The DNA sequence is: AAAGGTACCGAATTCACAGCATTGTACCCAGAGTCTGTCCCCAGACATTGCACCTGGCGCTGTGCGCCAATTCACAGCATTGTACCCAGAGTCTGTCCCCAGACATTGCACCTGGCGCTGTGCGCCAATTCACAGCATTGTACCCAGAGTCTGTCCCCAGACATTGCACCTGGCGCTGTGCGCCAATTCACAGCATTGTACCCAGAGTCTGTCCCCAGACATTGCACCTGGCGCTGTGGATCCGGTACCAAA.
Gene	*12 x MS2 binding sequence (12xMS2bs)*	(Bertrand et al., 1998b)		Amplified by PCR from the plasmid pLOX_HIS_MS2Lx12 gifted by Prof Jeffrey E. Gerst. The DNA sequences is: GATCCTAAGGTACCTAATTGCCTAGAAAACATGAGGATCACCCATGTCTGCAGGTCGACTCTAGAAAACATGAGGATCACCCATGTCTGCAGTATTCCCGGGTTCATTAGATCCTAAGGTACCTAATTGCCTAGAAAACATGAGGATCACCCATGT

				CTGCAGGTCGACTCTAGAAAACATGAGGATCACCCATGT CTGCAGTATTCCCGGGTTCATTAGATCCTAAGGTACCTA ATTGCCTAGAAAACATGAGGATCACCCATGTCTGCAGGT CGACTCCAGAAAACATGAGGATCACCCATGTCTGCAGTA TTCCCGGGTTCATTAGATCCTAAGGTACCTAATTGCCTA GAAAACATGAGGATCACCCATGTCTGCAGGTCGACTCTA GAAAACATGAGGATCACCCATGTCTGCAGTATTCCCGGG TTCATTAGATCCTAAGGTACCTAATTGCCTAGAAAACATG AGGATCACCCATGTCTGCAGGTCGACTCTAGAAAACATG AGGATCACCCATGTCTGCAGTATTCCCGGGTTCATTAGA TCCTAAGGTACCTAATTGCCTAGAAAACATGAGGATCAC CCATGTCTGCAGGTCGACTCCAGAAAACATGAGGATCAC CCATGTCTGCAGTATTCCCGGGTTCATTAGATC.
Gene	*Nuclear Localizing Signal (NLS)*	(Adam et al., 1989)		Tagged nucleotide sequences amplified by PCR. The DNA sequences is: CCAAAAAAAAAAAGAAAAGTT. The amino acid sequence is: PKKKRKV.
Gene	*Peroxisome Targeting Signal 1 (PTS1)*	(Kawaguchi et al., 2011)		Tagged nucleotide sequences amplified by PCR. The DNA sequence is: GCTAAATTA. The amino acid sequence is AKL.
Gene	*KAR2 signal sequence (KAR2ss)*	This study		Amplified by PCR from the *C. boidinii* genome. The sequence is:

				ATGTTTAAATTCAATCGTTCTTTTATAGCTTCTTTAGCTATATTATATTCTCTATTATTAATAATAGTACCTTTATTATCTCAACAAGCTCACGCTGAAGATGAA. The amino acid sequence is MFKFNRSFIASLAILYSLLLIIVPLLSQQAHAEDE.
Gene	*Retention sequence to the ER (HDEL)*	(Rose et al., 1989)		Tagged nucleotide sequences amplified by PCR. The sequence is: CACGATGAATTA. The amino acid sequence is HDEL.
Antibody	Anti-AOD (rabbit polyclonal)	(Sakai et al., 1996)		1:1000
Antibody	Anti-DAS (rabbit polyclonal)	(Sakai et al., 1996)		1:1000
Antibody	Anti-GAPDH (rabbit polyclonal)	GeneTex	GTX100118	1:5000
Antibody	Anti-βactin (mouse monoclonal)	Abcam	mAbcam 8224	1:1000
Antibody	Anti-IgG (H + L chain) mouse (goat polyclonal)	MBL	No. 330	1:10000

antibody	anti-rabbit-HRP (goat polyclonal)	Abcam	#7074	1:10000
Strain (*Escherichia coli*)	HST08	TaKaRa	Cat# 9128	
Plant ecotype (*Arabidopsis thaliana*)	Col-0	(Kawaguchi et al., 2011)		
Commercial assay or kit	In-Fusion HD cloning kit	TaKaRa	Cat# Z9648N	
Commercial assay or kit	T4 Polynucleotide Kinase	NEB	Cat# M0201S	
Commercial assay or kit	KOD FX Neo	TOYOBO	Cat# KFX-101	
Commercial assay or kit	Ligation convenience kit	Nippongene	Cat# 319-05961	

Commercial assay or kit	Wizard® Plus SV Minipreps DNA Purification Systems	Promega	Cat# A1330	
Commercial assay or kit	Wizard® SV Gel and PCR Clean-Up System	Promega	Cat# A9282	
Commercial assay or kit	Fast Yeast Transformation Kit	G-Bioscience s	Cat# GA005	
Commercial assay or kit	Rneay Mini Kit	QIAGEN	Cat# 74104	
Chemical compound, drug	Difco Yeast Nitrogen Base w/o Amino Acids	Becton Dickinson	Cat# 291040	
Chemical compound, drug	Bacto Yeast Extract	Becton Dickinson	Cat# 212750	

Chemical compound, drug	BD Bacto Peptone	Becton Dickinson	Cat# 211677	
Chemical compound, drug	BD Bacto Tryptone	Becton Dickinson	Cat# 211705	
Chemical compound, drug	Ampicillin sodium	WAKO	Cat# 012-23303	
Chemical compound, drug	Zeocin	Invitrogen	Cat# R250-01	
Chemical compound, drug	Blasticidin *S*, hydrochrolide	Funakoshi	Cat# KK-400	
Chemical compound, drug	5-fluoroorotidic acid	WAKO	Cat# 220141-70-8	
Chemical compound, drug	Cycloheximide	WAKO	Cat# 0034-11133	
Chemical compound, drug	Puromycin dihydrochloride	WAKO	Cat# 160-23151	

Chemical compound, drug	1,6-Hexanediol	Tokyo Chemical Industry	Cat# H0099	
Chemical compound, drug	Uracil	WAKO	Cat# 214-00061	
Chemical compound, drug	L-Leucine	WAKO	Cat# 124-00852	
Chemical compound, drug	L-Arginine	WAKO	Cat# 084-00682	
Chemical compound, drug	L-Histidine	WAKO	Cat# 015-04613	
Chemical compound, drug	Rhodamine-phalloidin	Thermo Fisher	Cat# R415	
Chemical compound, drug	Zymolyase-100T	Nacalai Tesque	Cat# 07665-55	
Chemical compound, drug	Hydrogen peroxide (35%)	Nacalai Tesque	Cat# 20779-65	

Chemical compound, drug	Sodium chloride	Nacalai Tesque	Cat# 31320-05	
Chemical compound, drug	DAPI solution	Nacalai Tesque	Cat# 19178-91	
Chemical compound, drug	Fiji	National Institutes of Health, NIH		
Software, algorithm	MetaMorph	Molecular Devices		
Software, algorithm	cellSense	Olympus		
Sequence-based reagent	FISH probes Probe_DAS_A	This study		Purchased from LGC Biosearch Technologies CCAGGATGACCACCTTCATATTGTTCAACTAAATCCAAGACATAACAACGGAATGCTCTCATTGTTAAATCATGGATATC
Sequence-based reagent	FISH probes Probe_DAS_B	This study		Purchased from LGC Biosearch Technologies GTTCCAATGCCTTGACAATAGTAGCAACATCTCTAGCACCATCTTCAACTTCAATAACATTCCAATTACAAGCTCTAAAC

Sequence-based reagent	FISH probes Probe_DAS_C	This study		Purchased from LGC Biosearch Technologies TGATTTTCAATTCTCTAATACCTTCTTCACCTAAAGCACTA CCATGAGCAGCACAATGATTTTGGAAAGCTGAATCAGTA
Sequence-based reagent	FISH probes Probe_DAS_D	This study		Purchased from LGC Biosearch Technologies GAACCAGCAATAACATTTGGAACATCTTTAGCTAATGCTC TAACCATAGCTCTAGCTGATGTTCTTGTTGCTGTATCTTC
Sequence-based reagent	FISH probes Probe_DAS_E	This study		Purchased from LGC Biosearch Technologies AACAGCTTGTTCTAATTCTGAACCAGCACCAATTAATTGA ATATCAGCATCTTTAGCATCTTCAAATACATAACCACCTC
Sequence-based reagent	qPCR primer RT-Act1-Fw	This study		TTGTCCCAATTTACGCTGG
Sequence-based reagent	qPCR primer RT-Act1-Rv	This study		CAGCAGTGGTGGAGAAAGTG
Sequence-based reagent	qPCR primer RT-AOD1-Fw	This study		TGCTGCTCCAGATTTCGATCC
Sequence-based reagent	qPCR primer RT-AOD1-Rv	This study		GGTTCACCAGCAAAACATTCC

Sequence-based reagent	qPCR primer RT-DAS1-Fw	This study		TGCAGCCCCAGCATTAAGAA
Sequence-based reagent	qPCR primer RT-DAS1-Rv	This study		GCAATAGGTTGATGTGTTGGTCC
Sequence-based reagent	qPCR primer RT-CbFLD1-fw	This study		GACCGATGGTGGTTGTGATTTC
Sequence-based reagent	qPCR primer RT-CbFLD1-rv	This study		GCGGCAACACCAATGATAACAG
Sequence-based reagent	qPCR primer Fw-TDH3-rtpcr1	This study		ACCACCGTTCACTCCATCACTGC
Sequence-based reagent	qPCR primer Rv-TDH3-rtpcr1	This study		CCGGAAGCAGTTCTACCACCTCTCC
Sequence-based reagent	qPCR primer RT-CbFDH1-Fw	This study		TTGTCTCTGTTGCTGAACACG
Sequence-based reagent	qPCR primer RT-CbFDH1-Rv	This study		TAGCGATAGCAGCAACCTCC
Sequence-based reagent	qPCR primer RT-CbFGH1-Fw-2	This study		AGGCATTTTGGCAACCATATGCAA

Sequence-based reagent	qPCR primer RT-CbFGH1-Rv-2	This study		CCAGCACCTGTACCGAAATCCC
Sequence-based reagent	qPCR primer RT-CbPMP20-Fw	This study		ACACCACCATGTACTGAACAAC
Sequence-based reagent	qPCR primer RT-CbPMP20-Rv	This study		CATCAGCTGCACCAAGCTC
Sequence-based reagent	qPCR primer RT-CbCTA1-Fw-2	This study		CGCCTTTTCCACCCAACGTA
Sequence-based reagent	qPCR primer RT-CbCTA1-Rv-2	This study		GCACCTTTGGCATGGACAAC

Yeast strains and culture conditions

Yeast strains used in this study are listed in Supplementary file Table S1. Cells were grown at 28ºC in the media described below. YPD (yeast extract peptone dextrose) medium consisted of 1% yeast extract, 2% bactopeptone and 2% glucose. Synthetic media were prepared with 0.67% yeast nitrogen base without amino acids and supplemented with one of the following carbon sources: 2% glucose for SD (synthetic dextrose), 2% ethanol for SE (synthetic ethanol) or 0.7% methanol for SM (synthetic methanol) medium. These media were supplemented with the appropriate amino acids (20 μg/mL uracil, 100 μg/mL leucine, 100 μg/mL arginine and/or 100 μg/mL histidine) and/or antibiotics (50 μg/mL zeocin or 100 μg/mL blasticidin) and/or 0.08% w/v of 5-fluoroorotidic acid (5-FOA), as necessary. The pH of SD, SE and SM media was adjusted to 6.0 with NaOH. Cell growth was monitored by measuring the optical density at 610 nm (OD_{610}). Solid media were prepared by the addition of 2% agar to the appropriate liquid media.

Escherichia coli HST08 premium competent cells (TaKaRa Bio Inc., Shiga, Japan) were used for gene cloning. *E. coli* was grown at 37°C on LB medium (1% Bacto tryptone, 0.5% Bacto yeast extract and 0.5% NaCl) in the presence of ampicillin (50 μg/mL).

DNA isolation and transformation

Plasmid DNA from *E. coli* was isolated using the Wizard® Plus SV Minipreps DNA Purification System (Promega, Madison, WI). Transformation of *E. coli* was carried out following the method of Dower et al (Dower et al., 1988). Genomic DNA from yeast was extracted using the method of Cryer et al (Cryer et al., 1975). Transformation of *C. boidinii* was performed using the Fast Yeast Transformation Kit (G-Biosciences, Maryland Heights, MO) or a modified lithium acetate method (Sakai & Tani, 1992), and *K. phaffii* transformation was conducted as previously described (Higgins & Cregg, 1998).

Plasmid construction

Primers used in this study are listed in Supplementary file Table S2, and plasmids used in this study are listed in Supplementary file Table S3. Details of the plasmid construction are described in Supplementary file.

Visualization of mRNAs in fixed cells

Fluorescence *in situ* hybridization (FISH) was performed using the method previously

described (McIsaac et al., 2013) with Stellaris® RNA FISH Probe (LGC Biosearch Technologies, Petaluma, CA). Custom oligonucleotide probes complementary to the target mRNA were designed with Cy5 conjugated at the 5′ end. Probe sequences are listed in Key Resources Table. Dried probes were dissolved in TE buffer (10 mM Tris-HCl, 1 mM EDTA, pH 7.0) and stored at −20°C before use.

Briefly, yeast cells were cultured in SM medium and harvested at 3 hours after the start of cultivation. Cells were then fixed with 35% formaldehyde at a final concentration of 3.5% (v/v), washed with fixation buffer (1.0 M Sorbitol, 0.1 M K_2HPO_4) and resuspended in fixation buffer supplemented with Zymolyase for spheroplastization. After washing with fixation buffer, cells were resuspended in 70% ethanol and stored at 4°C overnight. Subsequently, fixed cells were washed with SSC-formamide wash buffer, and then hybridized overnight at 37°C in hybridization buffer containing the Cy5-labelled probe at a final concentration of 12.5 μM. Finally, cells were resuspended in wash buffer, mounted on glass slides, and observed by fluorescence microscopy to determine the subcellular localization of target mRNAs based on Cy5 signal distribution.

Visualization of mRNAs in live cells

To visualize mRNAs in living cells, we employed both the U1A-based and MS2-based RNA systems. In the U1A system, the human U1A RNA-binding protein was used to tether the fluorescent protein Venus to target mRNAs (Chung & Takizawa, 2011). Four tandem repeats of the U1A binding sequence (U1Abs) were directly inserted into the 3' untranslated region (3'UTR) of the target genes at their endogenous genomic loci. The localization of these tagged mRNAs was monitored by co-expression of a fusion protein consisting of U1A and Venus with a nuclear localization signal (NLS) at its N terminus (NLS-U1A-Venus) (see Figure 2–figure supplement 2 for schematic diagram).

In parallel, the MS2 system was also used to visualize mRNAs where the bacteriophage-derived MS2 coat protein (MCP) was used to tether the fluorescent protein Cerulean to target mRNAs (Bertrand et al., 1998a). Twelve tandem repeats of the MS2 binding sequence (12xMS2L) were directly inserted into the 3'UTR sequences of the target genes at their endogenous genomic loci. The localization of these tagged mRNAs was monitored by co-expression of the NLS-MCP-Cerulean.

Fluorescence microscopy

Two microscopy systems were used for fluorescence imaging: a fluorescence microscope and a confocal laser scanning microscope.

Fluorescence microscopy was performed using the IX81 inverted fluorescence

microscope (Olympus, Tokyo, Japan) equipped with an XF52 filter set (Omega Optical Inc., Brattleboro, VT) suitable for detecting Cy5, DAPI, Rhodamine-Phalloidin and fluorescent proteins. Images were captured with a SenSys™ charged-coupled device (CCD) camera (PhotoMetrics, Tucson, AZ) and analyzed on MetaMorph software (Universal Imaging Corporation, Downingtown, PA), Fiji (Schindelin et al., 2012) and Adobe Photoshop (Adobe Inc., San Jose, CA). Scale bars in figures represent the indicated size.

Time-lapse imaging was performed using the IX83 inverted fluorescence microscope (Evident, Tokyo, Japan) equipped with an IX3-SSU motorized stage (Evident), a drift compensation module (IX3-ZDC, Evident) and a filter wheel unit (96A357 and MAC6000, Ludl Electronic Products Ltd., Hawthorne, NY, USA) suitable for detecting fluorescent proteins. Images were captured with ORCA-Fusion Digital CMOS camera (USB3.0 set, Hamamatsu Photonics, Hamamatsu, Japan) and analyzed on cellSens software (Evident) and Fiji. Cells were cultured under continuous medium flow using the CellASIC® ONIX2 Microfluidic System (Merck, Darmstadt, Germany) with the CellASIC® ONIX B04A-03 Microfluidic Bacteria Plate (Merck), according to the manufacturer's instructions. Images were acquired every 28 seconds for 20 cycles.

Confocal microscopy was conducted using the FV3000 confocal microscope (Olympus) equipped with six solid-state diode lasers (405, 445, 488, 514, 561 and 640 nm). The system utilizes high-numerical-aperture objectives, including UPLSAPO 100× (NA 1.35, silicone oil immersion; Olympus). Fluorescence signals were detected with high-sensitivity GaAsP detectors, allowing for the capture of faint signals with high signal-to-noise ratios. Venus fluorescence was excited at 488 nm and detected with a 500–600 nm emission filter, whereas Cerulean fluorescence was excited at 445 nm and detected with a 460–500 nm emission filter. Differential interference contrast (DIC) images were acquired using transmitted light with Nomarski optics. The images were captured and processed using cellSens software (Olympus), Fiji and Photoshop.

Morphometric and statistical analyses

Cell counts were analyzed from fluorescence microscopy images (n = 30 cells per biological replicate, with 3 biological replicates). In total, 90 cells were analyzed to quantify dot numbers and colocalization rates. Statistical significance was assessed using Welch's unpaired two-tailed t-test.

1,6-hexanediol treatment

1,6-hexanediol (HXD) treatment was performed using the method previously described

(Kroschwald et al., 2017). HXD disrupts weak hydrophobic interactions such as those involved in phase-separated biomolecular condensates. Cells were pre-cultured in SD medium for 12 hours and then transferred to SM medium. After 3 hours of methanol induction, 800 μL of cell culture was collected. Then, digitonin was added to a final concentration of 10 μg/mL, mixed gently and incubated for 5 minutes to mildly permeabilize the plasma membrane. Subsequently, 200 μL of 50% (v/v) HXD was added to achieve a final concentration of 10%. After a 1-minute incubation, cells were immediately subjected to fluorescence microscopy to assess the dissolution of condensates or subcellular structures.

Cycloheximide/puromycin treatment

Cells were pre-cultured in SD medium for 12 hours and then transferred to SM medium containing either cycloheximide (CHX) or puromycin (PMC) at a final concentration of 0.1 mg/mL. After the addition, cells were subjected to fluorescence microscopy at the indicated time points. CHX was used to stall ribosomes on mRNAs, preserving translation complexes, while PMC was used to release nascent peptides by causing premature termination. These treatments were used to examine the effects of translational inhibition.

Nuclear staining

After cultivation for the indicated time period, formaldehyde was added to the culture at a final concentration of 5% (v/v) to fix the cells. Following a 30-minute incubation, cells were harvested and washed twice with 1 mL of phosphate-buffered saline (PBS: 137 mM NaCl, 2.7 mM KCl, 10 mM Na_2HPO_4, 1.8 mM KH_2PO_4, pH 7.4). The fixed cells were then resuspended in 200μl of DAPI (4',6-diamidino-2-phenylindole) solution at a final concentration of 0.1 μg/mL. After 20 minutes of incubation, cells were then washed twice with 1 mL of PBS and were used for fluorescence microscopy.

Actinpatch staining

After cultivation for the indicated time, formaldehyde was added to the culture at a final concentration of 5% (v/v) to fix the cells. Following a 30-minute incubation, cells were harvested and washed three times with 1 mL of PBS. The fixed cells were then resuspended in 150 μL of PBS containing 3 μL of Rhodamine-Phalloidin and incubated for 2 hours at room temperature. After staining, cells were washed three times with 150 μL of PBS and used for fluorescence microscopy.

Preparation of cell-free extract and qRT-PCR analysis

Extraction of total RNA and cDNA synthesis were performed as previously described (Ohsawa et al., 2017) . qRT-PCR was performed with SYBR Premix Ex Taq (Takara Bio Inc.) using QuantStudio 1 Real-Time PCR System (Thermo Fisher Scientific, Waltham, MA). Transcript levels of all genes were normalized to *ACT1*. The primers for *ACT11*, *AOD1*, *DAS1*, *FLD1*, *FGH1*, *FDH1*, *CTA1* and *PMP20* are listed in the Key Resources Table.

Preparation of protein extracts from yeast cells and immunoblot analysis

Protein extracts from yeast cells and immunoblot analysis were prepared as previously described (Shiraishi et al., 2024). The primary antibody and secondary antibody used in this study were anti-AOD (rabbit polyclonal) (Sakai et al., 1996), anti-DAS (rabbit polyclonal) (Sakai et al., 1996), anti-GAPDH (GTX100118, rabbit polyclonal, GeneTex, Irvine, CA), anti-βactin (mAbcam 8224, mouse monoclonal, Abcam, Cambridge, UK), Anti-IgG (H + L chain) mouse (No. 330, goat polyclonal, MBL Co., Ltd., Tokyo, Japan) and anti-rabbit-HRP (#7074, goat polyclonal, Abcam).

Host plant growth conditions and yeast inoculation on plant leaves

A. thaliana plants were cultivated on mini-pots of cultivable lock-fiber (Nittobo, Tokyo, Japan) with Hoagland solution in growth chambers, as previously described (Kawaguchi et al., 2011). *C. boidinii* cells were cultured to OD_{610} = 1.0. To follow yeast proliferation on the leaves of *A. thaliana*, 1 µl of yeast cell suspension (OD_{610} = 0.5) was spotted onto the upper sides of the leaves. To observe Venus and/or Cerulean expression in *C. boidinii*, 5 µl of yeast suspension (OD_{610} = 0.5) was spotted onto the upper sides of the leaves. Then, the yeast cells were incubated on *A. thaliana* leaves until they were harvested for analysis.

Quantitation of yeast cell numbers on A. thaliana

After *C. boidinii* cells were inoculated on the leaves of *A. thaliana* for the indicated days, 5 leaves were collected. These leaves were placed in a 1.5 mL tube, and then, 100 µL of PBS was added per 10 mg of leaf and vortexed for 15 minutes. 20 µL of this collection sample was mixed with 20 µL of BD™ Liquid counting Beads (BD Biosciences) and 200 µL of PBS and the total volume was used for flow cytometry (FCM) analysis to count the cell population. Quantitation of yeast cell numbers was performed as previously described, using the FACSAria™ III Cell Sorter (Becton Dickinson, Franklin Lakes, NJ) (Katayama et al., 2025). Briefly, fluorescent channel and light scatter were set at log gain. The

forward scatter (FSC) was set at a photomultiplier tube (PMT) voltage of 2220 with a threshold of 200. The PMT voltages of side scatter (SSC) were set at 250 with a threshold of 200. Venus fluorescence was excited with a 488-nm laser and the emission at 530/30 nm was detected. Cells were counted referring to 2000 quantitative beads as standards. To ensure that FCM sorts Venus-labelled cells properly, we set gates for these labelled cells by using the Venus-labelled cells cultivated in SM medium. FACSDiva 8 software (Becton Dickinson) was used for data acquisition.

Data availability

All sequence data obtained in this study have been deposited in the DDBJ Sequence Read Archive. The accession numbers for the sequence data are LC889013 (*CbDCP2*), LC889015 (*CbKAR2*), LC889016 (*CERULEAN*), LC889017 (*BSD*^{r}), LC889018 (*U1A*) and LC889019 (*MS2*). All data generated or analyzed during this study are included in the manuscript and supporting files; Source Data files have been provided for Figures 1–5, and Figure 2–figure supplement 2, Figure 2–figure supplement 3, Figure 3–figure supplement 1, Figure 3–figure supplement 2, Figure 4–figure supplement 1, Figure 2–figure supplement 2, Figure 4–figure supplement 4, Figure 4–figure supplement 5, and Figure 5–figure supplement 1. These files contain the numerical data used to generate the figures. Figure 4–Source Data 2, Figure 3–figure supplement 1–Source Data 2, and Figure 4–figure supplement 4–Source Data 2 contain the original data of the images in each figure. The lists of yeast strains, plasmids and primers, along with details for plasmid construction, are provided in the Supplementary file.

Acknowledgments

We thank Shiori Katayama for technical assistance in the investigation of yeast proliferation using FCM; and Jeffrey E. Gerst for providing a plasmid harboring 12 repeats of the MS2 coat protein (MCP) binding sequence. This work was supported in part by KAKENHI Grants-in-Aid for Early-Career Scientists 22K14862 and 25K08894 (to KS), Grant in Aid for Scientific Research (B) 23K25056 and 25K03321 and Grant in Aid for Challenging Research (Exploratory) 16K15089 (to HY) from the Japan Society for the Promotion of Science, ACT-X Grant Number JPMJAX2118 (to KS), GteX Grant Number JPMJGX23B4 (to KS) and SPRING Grant Number JPMJSP2110 (to FS) from the Japan Science and Technology Agency, Noda Institute for Scientific Research Grant (to KS) and by the Program for the Development of Next-generation Leading Scientists with Global Insight (L-INSIGHT), sponsored by the Ministry of Education, Culture, Sports, Science and Technology (MEXT), Japan (to KS).

References

Adam, S. A., Lobl, T. J., Mitchell, M. A., & Gerace, L. (1989). Identification of specific binding proteins for a nuclear location sequence. *Nature*, *337*(6204), 276-279. https://doi.org/10.1038/337276a0

Amberg, D. C. (1998). Three-dimensional imaging of the yeast actin cytoskeleton through the budding cell cycle. *Mol Biol Cell*, *9*(12), 3259-3262. https://doi.org/10.1091/mbc.9.12.3259

Andrei, M. A., Ingelfinger, D., Heintzmann, R., Achsel, T., Rivera-Pomar, R., & Lührmann, R. (2005). A role for eIF4E and eIF4E-transporter in targeting mRNPs to mammalian processing bodies. *RNA*, *11*(5), 717-727. https://doi.org/10.1261/rna.2340405

Aronov, S., Gelin-Licht, R., Zipor, G., Haim, L., Safran, E., & Gerst, J. E. (2007). mRNAs encoding polarity and exocytosis factors are cotransported with the cortical endoplasmic reticulum to the incipient bud in *Saccharomyces cerevisiae*. *Mol Cell Biol*, *27*(9), 3441-3455. https://doi.org/10.1128/mcb.01643-06

Beattie, G. A., & Lindow, S. E. (1995). The secret life of foliar bacterial pathogens on leaves. *Annu Rev Phytopathol*, *33*, 145-172. https://doi.org/10.1146/annurev.py.33.090195.001045

Bertrand, E., Chartrand, P., Schaefer, M., Shenoy, S. M., Singer, R. H., & Long, R. M. (1998). Localization of *ASH1* mRNA particles in living yeast. *Mol Cell*, *2*(4), 437-445. https://doi.org/10.1016/s1097-2765(00)80143-4

Bhattacharyya, S. N., Habermacher, R., Martine, U., Closs, E. I., & Filipowicz, W. (2006). Relief of microRNA-mediated translational repression in human cells subjected to stress. *Cell*, *125*(6), 1111-1124. https://doi.org/10.1016/j.cell.2006.04.031

Brengues, M., Teixeira, D., & Parker, R. (2005). Movement of eukaryotic mRNAs between polysomes and cytoplasmic processing bodies. *Science*, *310*(5747), 486-489. https://doi.org/10.1126/science.1115791

Buchan, J. R. (2024). Stress granule and P-body clearance: Seeking coherence in acts of disappearance. *Semin Cell Dev Biol*, *159-160*, 10-26. https://doi.org/https://doi.org/10.1016/j.semcdb.2024.01.002

Buchan, J. R., Muhlrad, D., & Parker, R. (2008). P bodies promote stress granule assembly in *Saccharomyces cerevisiae*. *J Cell Biol*, *183*(3), 441-455. https://doi.org/10.1083/jcb.200807043

Cadete, R. M., Melo, M. A., Dussán, K. J., Rodrigues, R. C., Silva, S. S., Zilli, J. E., Vital, M. J., Gomes, F. C., Lachance, M. A., & Rosa, C. A. (2012). Diversity and physiological characterization of D-xylose-fermenting yeasts isolated from the

Brazilian Amazonian Forest. *PloS One*, *7*(8), e43135. https://doi.org/10.1371/journal.pone.0043135

Chung, S., & Takizawa, P. A. (2011). *In vivo* visualization of RNA using the U1A-based tagged RNA system. *Methods Mol Biol*, *714*, 221-235. https://doi.org/10.1007/978-1-61779-005-8_14

Cougot, N., Babajko, S., & Séraphin, B. (2004). Cytoplasmic foci are sites of mRNA decay in human cells. *J Cell Biol*, *165*(1), 31-40. https://doi.org/10.1083/jcb.200309008

Cryer, D. R., Eccleshall, R., & Marmur, J. (1975). Chapter 3 Isolation of Yeast DNA. In D. M. Prescott (Ed.), *Methods Cell Biol* (Vol. 12, pp. 39-44). Academic Press. https://doi.org/https://doi.org/10.1016/S0091-679X(08)60950-4

Dahan, N., Bykov, Y. S., Boydston, E. A., Fadel, A., Gazi, Z., Hochberg-Laufer, H., Martenson, J., Denic, V., Shav-Tal, Y., Weissman, J. S., Aviram, N., Zalckvar, E., & Schuldiner, M. (2022). Peroxisome function relies on organelle-associated mRNA translation. *Sci Adv*, *8*(2), eabk2141. https://doi.org/10.1126/sciadv.abk2141

Decker, C. J., & Parker, R. (2012). P-bodies and stress granules: possible roles in the control of translation and mRNA degradation. *Cold Spring Harb Perspect Biol*, *4*(9), a012286. https://doi.org/10.1101/cshperspect.a012286

Decker, C. J., Teixeira, D., & Parker, R. (2007). Edc3p and a glutamine/asparagine-rich domain of Lsm4p function in processing body assembly in *Saccharomyces cerevisiae*. *J Cell Biol*, *179*(3), 437-449. https://doi.org/10.1083/jcb.200704147

Dower, W. J., Miller, J. F., & Ragsdale, C. W. (1988). High efficiency transformation of *E. coli* by high voltage electroporation. *Nucleic Acids Res*, *16*(13), 6127-6145. https://doi.org/10.1093/nar/16.13.6127

Escalante, L. E., & Gasch, A. P. (2021). The role of stress-activated RNA-protein granules in surviving adversity. *RNA*, *27*(7), 753-762. https://doi.org/10.1261/rna.078738.121

Eulalio, A., Behm-Ansmant, I., Schweizer, D., & Izaurralde, E. (2007). P-body formation is a consequence, not the cause, of RNA-mediated gene silencing. *Mol Cell Biol*, *27*(11), 3970-3981. https://doi.org/10.1128/mcb.00128-07

Fall, R., & Benson, A. A. (1996). Leaf methanol — the simplest natural product from plants. *Trends Plant Sci*, *1*(9), 296-301. https://doi.org/https://doi.org/10.1016/S1360-1385(96)88175-0

Fundakowski, J., Hermesh, O., & Jansen, R. P. (2012). Localization of a subset of yeast mRNAs depends on inheritance of endoplasmic reticulum. *Traffic*, *13*(12), 1642-

1652. https://doi.org/10.1111/tra.12011
Gould, S. J., Keller, G. A., Hosken, N., Wilkinson, J., & Subramani, S. (1989). A conserved tripeptide sorts proteins to peroxisomes. *J Cell Biol*, *108*(5), 1657-1664. https://doi.org/10.1083/jcb.108.5.1657
Grousl, T., Ivanov, P., Frýdlová, I., Vasicová, P., Janda, F., Vojtová, J., Malínská, K., Malcová, I., Nováková, L., Janosková, D., Valásek, L., & Hasek, J. (2009). Robust heat shock induces eIF2alpha-phosphorylation-independent assembly of stress granules containing eIF3 and 40S ribosomal subunits in budding yeast, *Saccharomyces cerevisiae*. *J Cell Sci*, *122*(Pt 12), 2078-2088. https://doi.org/10.1242/jcs.045104
Gunasekera, T. S., & Sundin, G. W. (2006). Role of nucleotide excision repair and photoreactivation in the solar UVB radiation survival of *Pseudomonas syringae* pv. *syringae* B728a. *J Appl Microbiol*, *100*(5), 1073-1083. https://doi.org/10.1111/j.1365-2672.2006.02841.x
Higgins, D. R., & Cregg, J. M. (1998). *Pichia protocols* (Vol. 103). Springer.
Hutchins, M. U., & Klionsky, D. J. (2001). Vacuolar Localization of Oligomeric α-Mannosidase Requires the Cytoplasm to Vacuole Targeting and Autophagy Pathway Components in *Saccharomyces cerevisiae*. *J Biol Chem*, *276*(23), 20491-20498. https://doi.org/https://doi.org/10.1074/jbc.M101150200
Jacobs, J. L., Carroll, T. L., & Sundin, G. W. (2005). The role of pigmentation, ultraviolet radiation tolerance, and leaf colonization strategies in the epiphytic survival of phyllosphere bacteria. *Microb Ecol*, *49*(1), 104-113. https://doi.org/10.1007/s00248-003-1061-4
Jang, G. J., Yang, J. Y., Hsieh, H. L., & Wu, S. H. (2019). Processing bodies control the selective translation for optimal development of Arabidopsis young seedlings. *Proc Natl Acad Sci U S A*, *116*(13), 6451-6456. https://doi.org/10.1073/pnas.1900084116
Katayama, S., Shiraishi, K., Kaji, K., Kawabata, K., Tamura, N., Tani, A., Yurimoto, H., & Sakai, Y. (2025). Methanol chemoreceptor MtpA- and flagellin protein FliC-dependent methylotaxis contributes to the spatial colonization of PPFM in the phyllosphere. *ISME Communications*, *5*(1). https://doi.org/10.1093/ismeco/ycaf092
Kawaguchi, K., Yurimoto, H., Oku, M., & Sakai, Y. (2011). Yeast Methylotrophy and Autophagy in a Methanol-Oscillating Environment on Growing *Arabidopsis thaliana* Leaves. *PloS One*, *6*(9), e25257. https://doi.org/10.1371/journal.pone.0025257

Kedersha, N., & Anderson, P. (2009). Regulation of translation by stress granules and processing bodies. *Prog Mol Biol Transl Sci*, *90*, 155-185. https://doi.org/10.1016/s1877-1173(09)90004-7

Kedersha, N., Cho, M. R., Li, W., Yacono, P. W., Chen, S., Gilks, N., Golan, D. E., & Anderson, P. (2000). Dynamic shuttling of TIA-1 accompanies the recruitment of mRNA to mammalian stress granules. *J Cell Biol*, *151*(6), 1257-1268. https://doi.org/10.1083/jcb.151.6.1257

Kedersha, N., Stoecklin, G., Ayodele, M., Yacono, P., Lykke-Andersen, J., Fritzler, M. J., Scheuner, D., Kaufman, R. J., Golan, D. E., & Anderson, P. (2005). Stress granules and processing bodies are dynamically linked sites of mRNP remodeling. *J Cell Biol*, *169*(6), 871-884. https://doi.org/10.1083/jcb.200502088

Kroschwald, S., Maharana, S., Mateju, D., Malinovska, L., Nüske, E., Poser, I., Richter, D., & Alberti, S. (2015). Promiscuous interactions and protein disaggregases determine the material state of stress-inducible RNP granules. *Elife*, *4*, e06807. https://doi.org/10.7554/eLife.06807

Kroschwald, S., Maharana, S., & Simon, A. W. (2017). Hexanediol: a chemical probe to investigate the material properties of membrane-less compartments. Matters,

Lajoie, P., Moir, R. D., Willis, I. M., & Snapp, E. L. (2012). Kar2p availability defines distinct forms of endoplasmic reticulum stress in living cells. *Mol Biol Cell*, *23*(5), 955-964. https://doi.org/10.1091/mbc.E11-12-0995

Lavut, A., & Raveh, D. (2012). Sequestration of highly expressed mRNAs in cytoplasmic granules, P-bodies, and stress granules enhances cell viability. *PLoS Genet*, *8*(2), e1002527. https://doi.org/10.1371/journal.pgen.1002527

Lindow, S. E., & Brandl, M. T. (2003). Microbiology of the Phyllosphere. *Appl Environ Microbiol*, *69*(4), 1875-1883. https://doi.org/doi:10.1128/AEM.69.4.1875-1883.2003

Long, R. M., Elliott, D. J., Stutz, F., Rosbash, M., & Singer, R. H. (1995). Spatial consequences of defective processing of specific yeast mRNAs revealed by fluorescent in situ hybridization. *RNA*, *1*(10), 1071-1078.

Lui, J., Castelli, L. M., Pizzinga, M., Simpson, C. E., Hoyle, N. P., Bailey, K. L., Campbell, S. G., & Ashe, M. P. (2014). Granules harboring translationally active mRNAs provide a platform for P-body formation following stress. *Cell Rep*, *9*(3), 944-954. https://doi.org/10.1016/j.celrep.2014.09.040

McIsaac, R. S., Silverman, S. J., Parsons, L., Xu, P., Briehof, R., McClean, M. N., & Botstein, D. (2013). Visualization and Analysis of mRNA Molecules Using Fluorescence *In Situ* Hybridization in *Saccharomyces cerevisiae*. *J Vis Exp*(76),

e50382. https://doi.org/10.3791/50382

Morales-Polanco, F., Bates, C., Lui, J., Casson, J., Solari, C. A., Pizzinga, M., Forte, G., Griffin, C., Garner, K. E. L., Burt, H. E., Dixon, H. L., Hubbard, S., Portela, P., & Ashe, M. P. (2021). Core Fermentation (CoFe) granules focus coordinated glycolytic mRNA localization and translation to fuel glucose fermentation. *iScience*, *24*(2), 102069. https://doi.org/10.1016/j.isci.2021.102069

Morris, C., & Kinkel, L. (2002). Fifty years of phyllosphere microbiology: Significant contributions to research in related fields. *Phyllosphere microbiol*, 365-375.

Mota, M. N., Palma, M., & Sá-Correia, I. (2024). *Candida boidinii* isolates from olive curation water: a promising platform for methanol-based biomanufacturing. *AMB Express*, *14*(1), 93. https://doi.org/10.1186/s13568-024-01754-9

Nemecek-Marshall, M., MacDonald, R. C., Franzen, J. J., Wojciechowski, C. L., & Fall, R. (1995). Methanol Emission from Leaves (Enzymatic Detection of Gas-Phase Methanol and Relation of Methanol Fluxes to Stomatal Conductance and Leaf Development). *Plant Physiol*, *108*(4), 1359-1368. https://doi.org/10.1104/pp.108.4.1359

Nissan, T., Rajyaguru, P., She, M., Song, H., & Parker, R. (2010). Decapping activators in *Saccharomyces cerevisiae* act by multiple mechanisms. *Mol Cell*, *39*(5), 773-783. https://doi.org/10.1016/j.molcel.2010.08.025

Ohsawa, S., Yurimoto, H., & Sakai, Y. (2017). Novel function of Wsc proteins as a methanol-sensing machinery in the yeast *Pichia pastoris*. *Mol Microbiol*, *104*(2), 349-363. https://doi.org/https://doi.org/10.1111/mmi.13631

Oku, M., & Sakai, Y. (2016). Pexophagy in yeasts. *Biochim Biophys Acta, 1863*(5), 992-998. https://doi.org/https://doi.org/10.1016/j.bbamcr.2015.09.023

Parker, R., & Sheth, U. (2007). P bodies and the control of mRNA translation and degradation. *Mol Cell*, *25*(5), 635-646. https://doi.org/10.1016/j.molcel.2007.02.011

Pilaz, L. J., Liu, J., Joshi, K., Tsunekawa, Y., Musso, C. M., D'Arcy, B. R., Suzuki, I. K., Alsina, F. C., Kc, P., Sethi, S., Vanderhaeghen, P., Polleux, F., & Silver, D. L. (2023). Subcellular mRNA localization and local translation of Arhgap11a in radial glial progenitors regulates cortical development. *Neuron*, *111*(6), 839-856.e835. https://doi.org/10.1016/j.neuron.2023.02.023

Reid, D. W., & Nicchitta, C. V. (2015). Diversity and selectivity in mRNA translation on the endoplasmic reticulum. *Nat Rev Mol Cell Biol*, *16*(4), 221-231. https://doi.org/10.1038/nrm3958

Riggs, C. L., Kedersha, N., Ivanov, P., & Anderson, P. (2020). Mammalian stress granules

and P bodies at a glance. *J Cell Sci*, *133*(16). https://doi.org/10.1242/jcs.242487

Ripin, N., & Parker, R. (2023). Formation, function, and pathology of RNP granules. *Cell*, *186*(22), 4737-4756. https://doi.org/10.1016/j.cell.2023.09.006

Rose, M. D., Misra, L. M., & Vogel, J. P. (1989). KAR2, a karyogamy gene, is the yeast homolog of the mammalian BiP/GRP78 gene. *Cell*, *57*(7), 1211-1221. https://doi.org/10.1016/0092-8674(89)90058-5

Ruinen, J. (1956). Occurrence of Beijerinckia Species in the 'Phyllosphere'. *Nature*, *177*(4501), 220-221. https://doi.org/10.1038/177220a0

Sakai, Y., Koller, A., Rangell, L. K., Keller, G. A., & Subramani, S. (1998). Peroxisome degradation by microautophagy in *Pichia pastoris*: identification of specific steps and morphological intermediates. *J Cell Biol*, *141*(3), 625-636. https://doi.org/10.1083/jcb.141.3.625

Sakai, Y., Saiganji, A., Yurimoto, H., Takabe, K., Saiki, H., & Kato, N. (1996). The absence of Pmp47, a putative yeast peroxisomal transporter, causes a defect in transport and folding of a specific matrix enzyme. *J Cell Biol*, *134*(1), 37-51. https://doi.org/10.1083/jcb.134.1.37

Sakai, Y., & Tani, Y. (1992). Directed mutagenesis in an asporogenous methylotrophic yeast: cloning, sequencing, and one-step gene disruption of the 3-isopropylmalate dehydrogenase gene (LEU2) of *Candida boidinii* to derive doubly auxotrophic marker strains. *J Bacteriol*, *174*(18), 5988-5993. https://doi.org/10.1128/jb.174.18.5988-5993.1992

Sasano, Y., Yurimoto, H., Yanaka, M., & Sakai, Y. (2008). Trm1p, a Zn(II)2Cys6-type transcription factor, is a master regulator of methanol-specific gene activation in the methylotrophic yeast *Candida boidinii. Eukaryot Cell*, *7*(3), 527-536. https://doi.org/10.1128/ec.00403-07

Schindelin, J., Arganda-Carreras, I., Frise, E., Kaynig, V., Longair, M., Pietzsch, T., Preibisch, S., Rueden, C., Saalfeld, S., Schmid, B., Tinevez, J. Y., White, D. J., Hartenstein, V., Eliceiri, K., Tomancak, P., & Cardona, A. (2012). Fiji: an open-source platform for biological-image analysis. *Nat Methods*, *9*(7), 676-682. https://doi.org/10.1038/nmeth.2019

Schneider-Poetsch, T., Ju, J., Eyler, D. E., Dang, Y., Bhat, S., Merrick, W. C., Green, R., Shen, B., & Liu, J. O. (2010). Inhibition of eukaryotic translation elongation by cycloheximide and lactimidomycin. *Nature Chemical Biology*, *6*(3), 209-217. https://doi.org/10.1038/nchembio.304

Scott, S. V., Baba, M., Ohsumi, Y., & Klionsky, D. J. (1997). Aminopeptidase I is targeted to the vacuole by a nonclassical vesicular mechanism. *J Cell Biol*, *138*(1), 37-44.

https://doi.org/10.1083/jcb.138.1.37
Shiraishi, K., Arima, Y., Nakamura, M., Nakatsuji, T., Oku, M., & Sakai, Y. (2024). A novel fluorescence-activated cell sorting (FACS)-based screening identified *ATG14*, the gene required for pexophagy in the methylotrophic yeast. *FEMS Yeast Res*, *24*. https://doi.org/10.1093/femsyr/foae022
Shiraishi, K., Hioki, T., Habata, A., Yurimoto, H., & Sakai, Y. (2018). Yeast Hog1 proteins are sequestered in stress granules during high-temperature stress. *J Cell Sci*, *131*(1). https://doi.org/10.1242/jcs.209114
Shiraishi, K., Oku, M., Kawaguchi, K., Uchida, D., Yurimoto, H., & Sakai, Y. (2015). Yeast nitrogen utilization in the phyllosphere during plant lifespan under regulation of autophagy. *Sci Rep*, *5*(1), 9719. https://doi.org/10.1038/srep09719
Singer-Krüger, B., & Jansen, R. P. (2014). Here, there, everywhere. mRNA localization in budding yeast. *RNA Biol*, *11*(8), 1031-1039. https://doi.org/10.4161/rna.29945
Sorenson, R., & Bailey-Serres, J. (2014). Selective mRNA sequestration by OLIGOURIDYLATE-BINDING PROTEIN 1 contributes to translational control during hypoxia in Arabidopsis. *Proc Natl Acad Sci U S A*, *111*(6), 2373-2378. https://doi.org/10.1073/pnas.1314851111
Standart, N., & Weil, D. (2018). P-Bodies: Cytosolic Droplets for Coordinated mRNA Storage. *Trends Genet*, *34*(8), 612-626. https://doi.org/10.1016/j.tig.2018.05.005
Swisher, K. D., & Parker, R. (2010). Localization to, and effects of Pbp1, Pbp4, Lsm12, Dhh1, and Pab1 on stress granules in *Saccharomyces cerevisiae*. *PloS One*, *5*(4), e10006. https://doi.org/10.1371/journal.pone.0010006
Takizawa, P. A., & Vale, R. D. (2000). The myosin motor, Myo4p, binds Ash1 mRNA via the adapter protein, She3p. *Proc Natl Acad Sci U S A*, *97*(10), 5273-5278. https://doi.org/10.1073/pnas.080585897
Tani, Y., Sakai, Y., & Yamada, H. (1985). Isolation and Characterization of a Mutant of a Methanol Yeast, *Candida boidinii* S2, with Higher Formaldehyde Productivity. *Agric Biol Chem*, *49*(9), 2699-2706. https://doi.org/10.1080/00021369.1985.10867154
Teixeira, D., & Parker, R. (2007). Analysis of P-Body Assembly in *Saccharomyces cerevisiae*. *Mol Biol Cell*, *18*(6), 2274-2287. https://doi.org/10.1091/mbc.e07-03-0199
Tishinov, K., & Spang, A. (2021). The mRNA decapping complex is buffered by nuclear localization. *J Cell Sci*, *134*(18). https://doi.org/10.1242/jcs.259156
Vorholt, J. A. (2012). Microbial life in the phyllosphere. *Nat Rev Microbiol*, *10*(12), 828-840. https://doi.org/10.1038/nrmicro2910

Wang, C., Schmich, F., Srivatsa, S., Weidner, J., Beerenwinkel, N., & Spang, A. (2018). Context-dependent deposition and regulation of mRNAs in P-bodies. *eLife*, *7*, e29815. https://doi.org/10.7554/eLife.29815

Wylin, T., Baes, M., Brees, C., Mannaerts, G. P., Fransen, M., & Van Veldhoven, P. P. (1998). Identification and characterization of human PMP34, a protein closely related to the peroxisomal integral membrane protein PMP47 of *Candida boidinii*. *Eur J Biochem*, *258*(2), 332-338. https://doi.org/https://doi.org/10.1046/j.1432-1327.1998.2580332.x

Yurimoto, H., Lee, B., Yasuda, F., Sakai, Y., & Kato, N. (2004). Alcohol dehydrogenases that catalyse methyl formate synthesis participate in formaldehyde detoxification in the methylotrophic yeast *Candida boidinii*. *Yeast*, *21*(4), 341-350. https://doi.org/https://doi.org/10.1002/yea.1101

Yurimoto, H., Oku, M., & Sakai, Y. (2011). Yeast methylotrophy: metabolism, gene regulation and peroxisome homeostasis. *Int J Microbiol*, *2011*, 101298. https://doi.org/10.1155/2011/101298

Yurimoto, H., Shiraishi, K., & Sakai, Y. (2021). Physiology of Methylotrophs Living in the Phyllosphere. *Microorganisms*, *9*(4), 809. https://www.mdpi.com/2076-2607/9/4/809

Zhang, B., Butler, A. M., Shi, Q., Xing, S., & Herman, P. K. (2018). P-Body Localization of the Hrr25/Casein Kinase 1 Protein Kinase Is Required for the Completion of Meiosis. *Mol Cell Biol*, *38*(17). https://doi.org/10.1128/mcb.00678-17

Zheng, D., Ezzeddine, N., Chen, C. Y., Zhu, W., He, X., & Shyu, A. B. (2008). Deadenylation is prerequisite for P-body formation and mRNA decay in mammalian cells. *J Cell Biol*, *182*(1), 89-101. https://doi.org/10.1083/jcb.200801196

Zipor, G., Haim-Vilmovsky, L., Gelin-Licht, R., Gadir, N., Brocard, C., & Gerst, J. E. (2009). Localization of mRNAs coding for peroxisomal proteins in the yeast, *Saccharomyces cerevisiae*. *Proc Natl Acad Sci U S A*, *106*(47), 19848-19853. https://doi.org/10.1073/pnas.0910754106

Figures

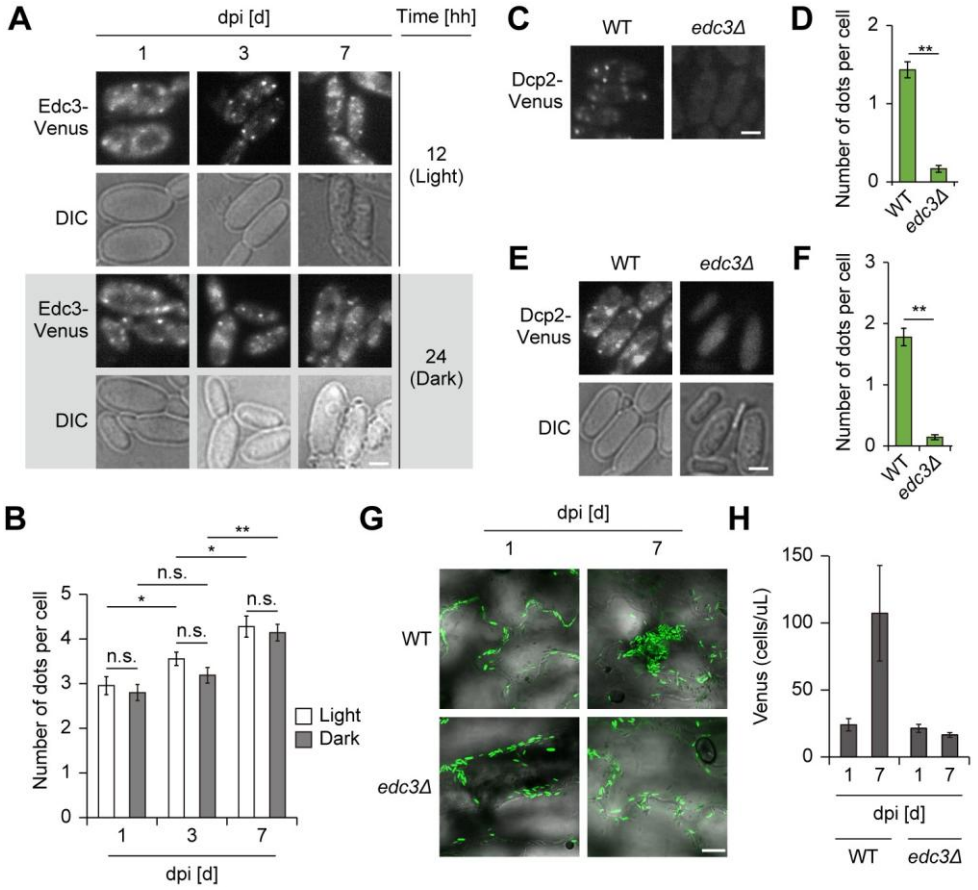

Figure 1. Formation and significance of yeast P-bodies on *A. thaliana* leaves.

(**A**) P-body formation in the WT strain on growing *Arabidopsis* leaves. Edc3-Venus fusion protein was expressed under the control of the native *EDC3* promoter as a marker. The strain was spotted on leaves, collected from the leaves at the indicated day/time post-inoculation and observed by a fluorescence microscope. DIC: differential interference contrast. Bar, 2 µm. dpi, days post-inoculation.

(**B**) Quantification of Edc3-Venus dot formation detected in (**A**). Cell count analysis was performed on fluorescence microscopy images (n = 30, n: number of cells analyzed; b = 3, b: biological replicates; total = 90 cells). The number of dots is presented as mean ± standard error (SE) of 90 cells. Asterisks indicate statistical significance: * $p < 0.05$; ** $p < 0.01$; n.s. means not significant.

(**C**) P-body formation in the WT and *edc3Δ* strains on SM media. Dcp2-Venus fusion protein was expressed under the control of the native *DCP2* promoter as a marker. The strains grown on SM medium were collected for microscopic observation. Bar, 2 µm.

(**D**) Quantification of Dcp2-Venus dot formation detected in (**C**). Cell count analysis was

performed on fluorescence microscopy images (n = 30, n: number of cells analyzed; b = 3, b: biological replicates; total = 90 cells). The number of dots is presented as mean ± standard error (SE) of 90 cells. Asterisks indicate statistical significance: ** $p < 0.01$.

(**E**) P-body formation in the WT and *edc3Δ* strains on growing *Arabidopsis* leaves. The strains expressing Dcp2-Venus were spotted on leaves and collected 4 hours after inoculation for microscopic observation. Bar, 2 μm.

(**F**) Quantification of Dcp2-Venus dot formation detected in (**E**).

Cell count analysis was performed on fluorescence microscopy images (n = 30, n: number of cells analyzed; b = 3, b: biological replicates; total = 90 cells). The number of dots is presented as mean ± SE of 90 cells. Asterisks indicate statistical significance: ** $p < 0.01$.

(**G**) Confocal microscope images of the Venus-labeled WT and *edc3Δ* strains on growing *Arabidopsis* leaves. Venus fluorescent protein was expressed under the control of the constitutive *ACT1* promoter. The strains were spotted on leaves and observed at the indicated days post-inoculation (dpi). Merged images of differential interference contrast (DIC) and Venus are depicted. Bar, 20 μm.

(**H**) Quantification of *C. boidinii* cell populations on *A. thaliana* leaves by flowcytometry (FCM). The leaves onto which the strains were inoculated were retrieved at the indicated days post-inoculation (dpi) and were subjected to FCM for counting the cell population expressing Venus. Values are indicated as mean ± SE of four biological replicates.

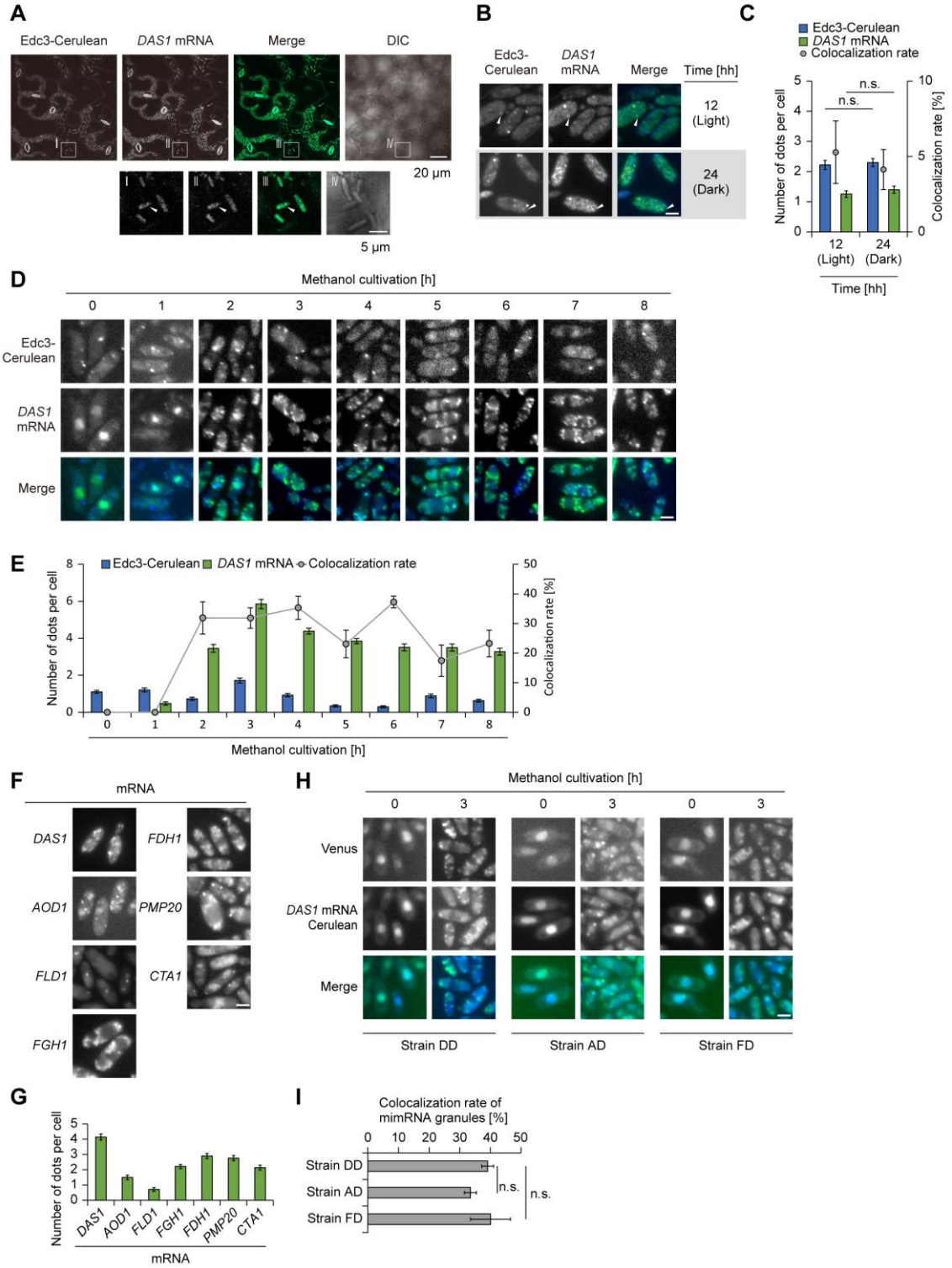

Figure 2. Intracellular dynamics of P-bodies and mimRNAs on methanol growth conditions.

(**A**) Confocal microscopy images of the WT strain expressing Edc3-Cerulean and Venus-tagged *DAS1* mRNA (strain Edc3-C/DAS1m-V) on growing *Arabidopsis* leaves. The

strain was spotted on the leaves and observed 4 hours after inoculation. Squares I, II, III and VI were enlarged. Merged images were generated by combining Venus and Cerulean fluorescence images. White arrows indicate colocalization of Edc3-Cerulean and Venus-tagged *DAS1* mRNA dots. The lengths of the bars are indicated in the images. DIC: differential interference contrast.

(**B**) Fluorescence microscopy images of strain Edc3-C/DAS1m-V on growing *Arabidopsis* leaves. The strain, spotted on leaves, was collected for observation from the leaf surface 4 hours after inoculation during both the light and dark periods. Merged images were generated by combining Venus and Cerulean fluorescence images. White arrows indicate colocalization of Edc3-Cerulean and Venus-tagged *DAS1* mRNA dots. Bar, 2 μm.

(**C**) Quantification of dot formation of Edc3-Venus and Venus-tagged *DAS1* mRNA and their colocalization detected in (**B**). Cell count analysis was performed on fluorescence microscopy images (n = 30, n: number of cells analyzed; b = 3, b: biological replicates; total = 90 cells). The number of dots is presented as the mean ± SE of 90 cells, and colocalization rates are shown as mean ± SE from three biological replicates (n = 30 cells per replicate). n.s. means not statistically significant.

(**D**) Time-course analysis of the intracellular localization of P-bodies and mimRNAs in strain Edc3-C/DAS1m-V during methanol induction. The strain grown on an SD medium was transferred to SM medium and collected at the indicated time points for fluorescence microscopy. Merged images were generated by combining Venus and Celurean fluorescence images. Bar, 2 μm.

(**E**) Quantification of dot formation of Edc3-Venus and Venus-tagged *DAS1* mRNA and their colocalization detected in (**D**). Cell count analysis was performed on fluorescence microscopy images (n = 30, n: number of cells analyzed; b = 3, b: biological replicates; total = 90 cells). The number of dots is presented as mean ± SE of 90 cells and colocalization rates are shown as mean ± SE from three biological replicates (n = 30 cells per replicate).

(**F**) Fluorescence microscopy images of the strains visualizing *DAS1*, *AOD1*, *FLD1*, *FGH1*, *FDH1*, *PMP20* and *CTA1* mRNAs. The strains grown on an SD medium were transferred to SM medium and incubated for 3 hours before fluorescence microscopy. Bar, 2 μm.

(**G**) Quantification of mimRNA granule formation detected in (**F**). Cell count analysis was performed on fluorescence microscopy images (n = 30, n: number of cells analyzed; b = 3, b: biological replicates; total = 90 cells). The number of dots is presented as mean ± SE of 90 cells.

(**H**) Intracellular localization of multiple mimRNAs during methanol induction. In strain DD, *DAS1* mRNA was visualized by the Venus-tagged U1A-based RNA system and Cerulean-tagged MS2-based RNA system. In strain AD and strain FD, *AOD1* or *FLD1* mRNA was visualized by Venus-tagged U1A-based RNA system and *DAS1* mRNA by Cerulean-tagged MS2-based RNA system. Merged images were generated by combining Venus and Cerulean fluorescence images. Bar, 2 μm.

(**I**) Quantification of the colocalization of the multiple mimRNA granules detected in (**H**). Cell count analysis was performed on fluorescence microscopy images (n = 30, n: number of cells analyzed; b = 3, b: biological replicates; total = 90 cells). The number of dots is presented as mean ± SE of 90 cells. n.s. means not statistically significant.

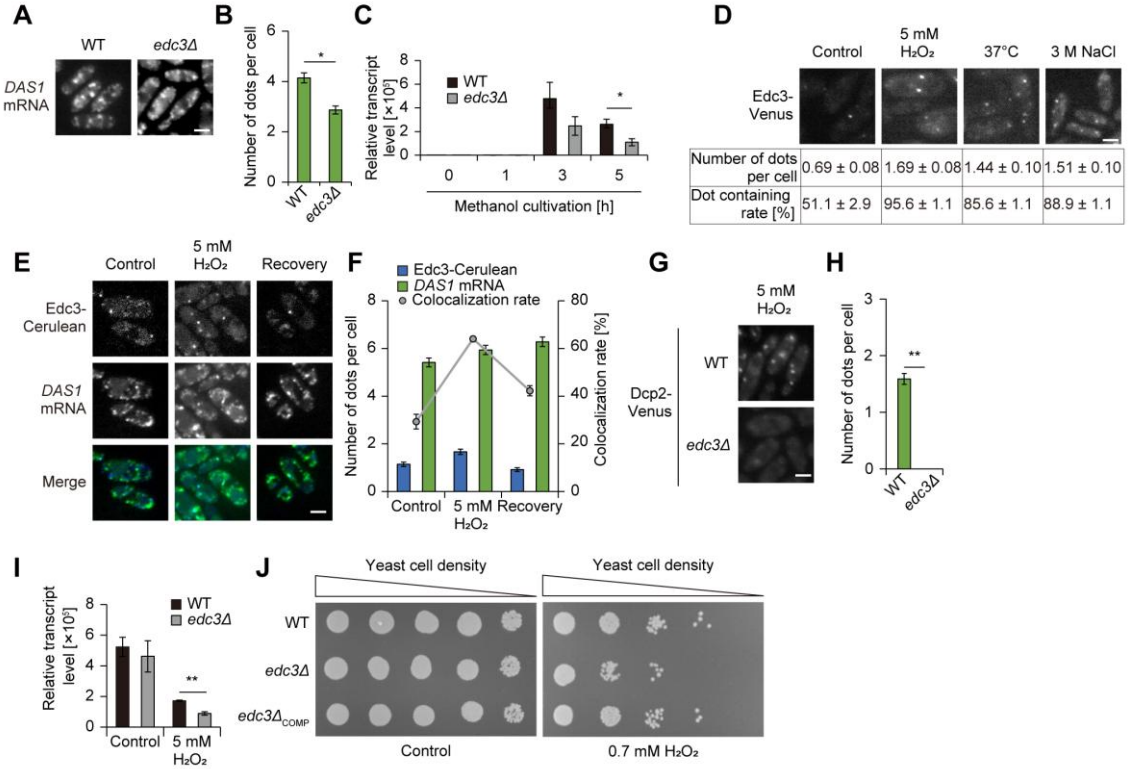

Figure 3. Role of P-bodies on post-transcriptional regulation of mimRNAs.

(**A**) Dot formation of Venus-tagged *DAS1* mRNA in the WT and *edc3Δ* strains on SM medium. The strains grown on an SD medium were transferred to SM medium and incubated for 3 hours before fluorescence microscopy. Bar, 2 µm.

(**B**) Quantification of Venus-tagged *DAS1* mRNA dot formation detected in (**A**). Cell count analysis was performed on fluorescence microscopy images (n = 30, n: number of cells analyzed; b = 3, b: biological replicates; total = 90 cells). The number of dots is presented as mean ± SE of 90 cells. Asterisks indicate statistical significance: * $p < 0.05$.

(**C**) Relative transcript levels of *DAS1* mRNA in the WT and *edc3Δ* strains on SM medium. Values are indicated as mean ± SE of three biological replicates. Statistical significance between the WT and *edc3Δ* strains were assessed. Asterisks indicate statistical significance: * $p < 0.05$.

(**D**) P-body formation under stress conditions. Strain Edc3-V was exposed to oxidative stress with 5 mM H_2O_2, heat shock at 37 degrees or salt stress with 3 M NaCl for 1 hour before microscopic observation. Cell count analysis was performed on fluorescence microscopy images (n = 30, n: number of cells analyzed; b = 3, b: biological replicates; total = 90 cells). The number of dots is presented as mean ± SE of 90 cells, and the proportion of cells containing at least one dot (dot containing rate) are shown as mean ±

SE from three biological replicates (n = 30 cells per replicate). Bar, 2μm.

(**E**) Fluorescence microscopy images of strain Edc3-C/DAS1m-V during oxidative stress and recovery from the stress. The strain incubated on an SM medium was treated with 5 mM H_2O_2 for 1 hour and then transferred to an SM medium. Merged images were generated by combining Venus and Cerulean fluorescence images. Bar, 2 μm.

(**F**) Quantification of dot formation of Edc3-Venus and Venus-tagged *DAS1* mRNA and their colocalization detected in (**E**). Cell count analysis was performed on fluorescence microscopy images (n = 30, n: number of cells analyzed; b = 3, b: biological replicates; total = 90 cells). The number of dots is presented as mean ± SE of 90 cells and colocalization rates are shown as mean ± SE from three biological replicates (n = 30 cells per replicate).

(**G**) P-body formation in the WT and *edc3Δ* strains expressing Dcp2-Venus under oxidative stress. The strains grown on SM medium were treated with 5 mM H_2O_2 for 1 hour and collected for microscopic observation.

(**H**) Quantification of Dcp2-Venus dot formation detected in (**I**). Cell count analysis was performed on fluorescence microscopy images (n = 30, n: number of cells analyzed; b = 3, b: biological replicates; total = 90 cells). The number of dots is presented as mean ± SE of 90 cells. Asterisks indicate statistical significance: ** $p < 0.01$.

(**I**) Relative transcript level of *DAS1* mRNA in the WT and *edc3Δ* strains on SM medium under oxidative stress. The strain was incubated on SM medium for 3 hours and then treated with 5 mM H_2O_2 for 1 hour. Transcript levels of all genes were first normalized to *ACT1* and then expression levels were calculated relative to samples collected at 0 h of methanol cultivation. In the graph, the sample collected at 3 h is labeled as "Control" for comparison. Values are indicated as mean ± SE of three biological replicates. Statistical significance between the WT and *edc3Δ* strains was assessed. Asterisks indicate statistical significance: ** $p < 0.01$.

(**J**) Growth assay of cells cultured under oxidative stress conditions. Cells were grown to early log phase, adjusted to OD_{610}=1, and 3 μL of tenfold serial dilutions were dropped onto SM plates with or without 0.7 mM H_2O_2. Subsequently, the SM plates were incubated at 28°C. Cell growth was analyzed after 2 days. Growth of the wild-type (WT), *edc3Δ,* and *edc3Δ* expressing Edc3-Venus (*edc3Δ*$_{COMP}$) under the native promoter was compared.

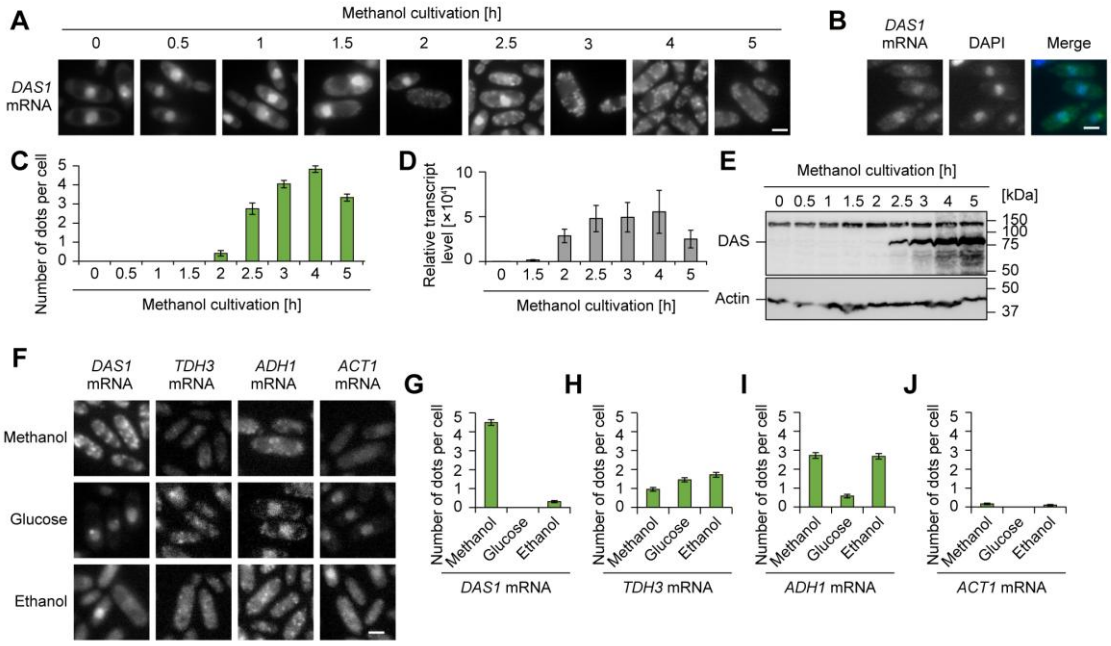

Figure 4. Regulation of mimRNA granule formation.

(**A**) Time-course analysis of the intracellular localization of Venus-tagged *DAS1* mRNA during methanol induction. The strain grown on an SD medium was transferred to SM medium and incubated for up to 5 hours and collected at indicated time points. Bar, 2 µm.

(**B**) Nuclear localization of Venus-tagged *DAS1* mRNA. The strain grown on an SD medium was collected for fluorescence microscopy. A merged image was generated by combining Venus and DAPI fluorescence images. Bar, 2 µm.

(**C**) Quantification of dot formation of Venus-tagged *DAS1* mRNA detected in (**A**). Cell count analysis was performed on fluorescence microscopy images (n = 30, n: number of cells analyzed; b = 3, b: biological replicates; total = 90 cells). The number of dots is presented as mean ± SE of 90 cells.

(**D**) Relative transcript level of *DAS1* mRNA in the WT strain during methanol induction. Values are indicated as the mean ± SE of three biological replicates.

(**E**) Immunoblot analysis of DAS in the WT strain during methanol induction. The expected molecular weight of DAS is 78.2 kDa.

(**F**) Fluorescence microscopy images of the strains visualizing *DAS1*, *TDH3*, *ADH1* and *ACT1* mRNAs during cultivation on various carbon sources. The strains grown on an SD medium were transferred to either SM, SD or SE medium and incubated for 3 hours. Bar, 2 µm.

(**G-J**) Quantification of mRNA dot formation detected in (**F**). Cell count analysis was performed on fluorescence microscopy images (n = 30, n: number of cells analyzed; b

= 3, b: biological replicates; total = 90 cells). The number of dots is presented as mean ± SE of 90 cells. (**G**) *DAS1* mRNA, (**H**) *TDH3* mRNA, (**I**) *ADH1* mRNA and (**J**) *ACT1* mRNA.

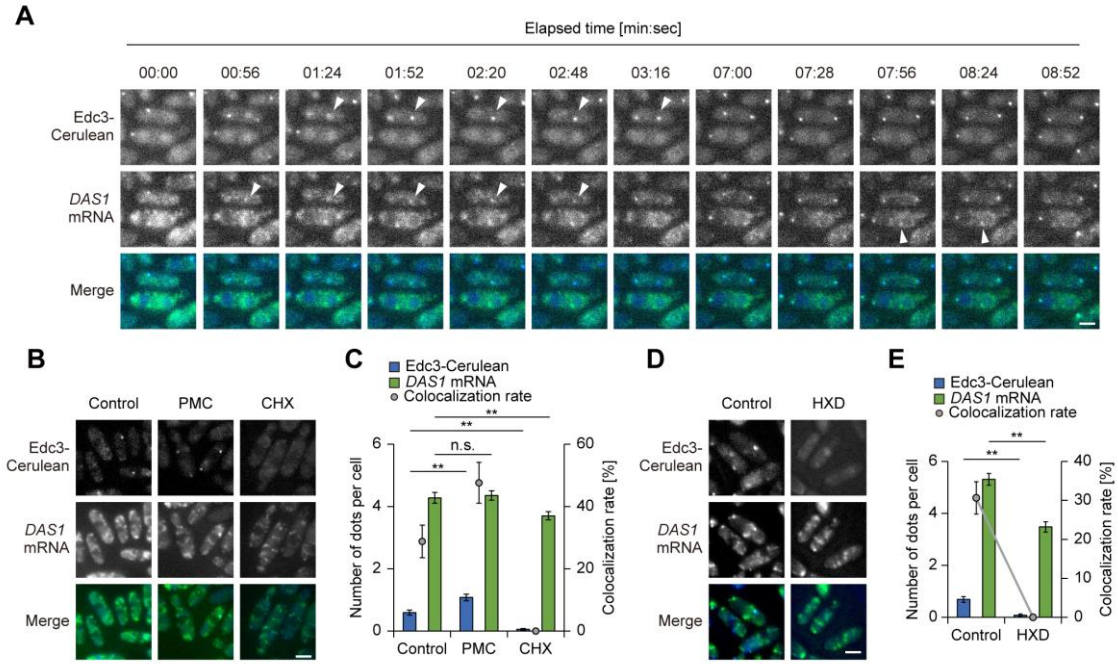

Figure 5. Properties of mimRNA granules.

(**A**) Time-lapse images of strain Edc3-C/DAS1m-V under methanol-grown conditions. Twelve images extracted at the indicated time points are shown as a video (see also Figure 5–video 1). Merged images were generated by combining Venus and Cerulean fluorescence images. White arrows indicate the dynamic properties of Edc3-Cerulean and Venus-tagged *DAS1* mRNA dots. A new Venus-tagged *DAS1* mRNA dot appeared at 56 seconds in the video, which colocalized with an Edc3-Cerulean dot from 1 min 24 s to 2 min 48 s, and disappeared at 3 min 16 s, while the Edc3-Cerulean dots remained. At 7 min 56 s, a Venus-tagged *DAS1* mRNA dot appeared without colocalizing with a P-body; this granule remained at the same site at 8 min 24 s but disappeared at 8 min 52 s. Bar, 2 μm.

(**B**) Fluorescence microscopy images of strain Edc3-C/DAS1m-V after treatment with protein synthesis inhibitors. The strain incubated on an SM medium was treated with either 0.1 mg/mL cycloheximide (CHX) or 0.1 mg/mL puromycin (PMC) before microscopic observation. Merged images were generated by combining Venus and Cerulean fluorescence images. Bar, 2 μm.

(**C**) Quantification of dot formation of Edc3-Venus and Venus-tagged *DAS1* mRNA and their colocalization detected in (**B**). Cell count analysis was performed on fluorescence microscopy images (n = 30, n: number of cells analyzed; b = 3, b: biological replicates; total = 90 cells). The number of dots is presented as mean ± SE of 90 cells and colocalization rates are shown as mean ± SE from three biological replicates (n = 30 cells

per replicate). Asterisks indicate statistical significance. ** $p < 0.01$. n.s. means not significant.

(**D**) Fluorescence microscopy images of strain Edc3-C/DAS1m-V after treatment with 1,6-hexandiol (HXD). The strain incubated on an SM medium was treated with 10% HXD before microscopic observation. Merged images were generated by combining Venus and Cerulean fluorescence images. Bar, 2 μm.

(**E**) Quantification of dot formation of Edc3-Venus and Venus-tagged *DAS1* mRNA and their colocalization detected in (**D**). Cell count analysis was performed on fluorescence microscopy images (n = 30, n: number of cells analyzed; b = 3, b: biological replicates; total = 90 cells). The number of dots is presented as mean ± SE of 90 cells and colocalization rates are shown as mean ± SE from three biological replicates (n = 30 cells per replicate). Asterisks indicate statistical significance. ** $p < 0.01$.

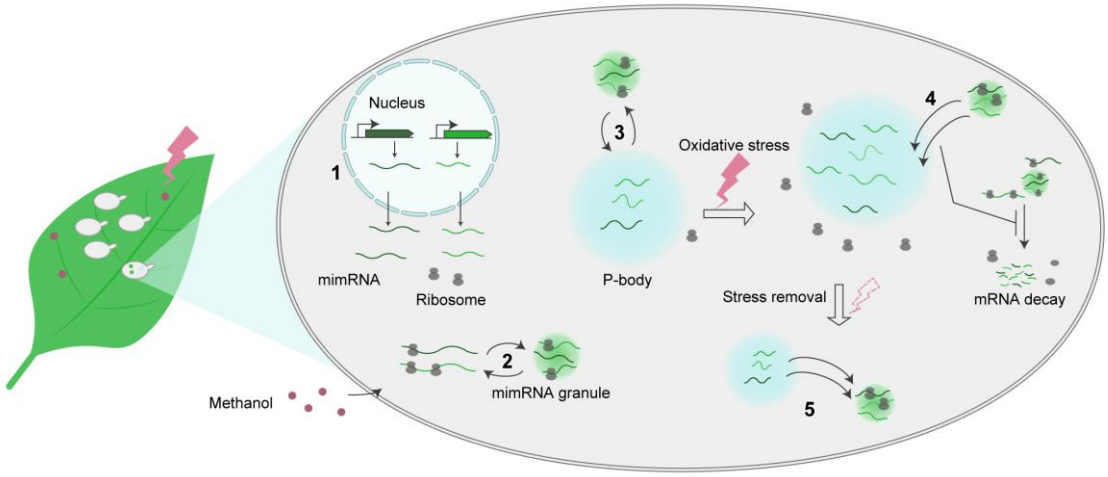

Figure 6. Schematic image illustrating the role of yeast P-bodies in the post-transcriptional regulation of methanol-induced genes in the phyllosphere.

On *A. thaliana* leaves, *C. boidinii* assimilates methanol as the carbon source while adapting to environmental stresses. In this leaf environment, P-bodies regulate methanol-induced genes post-transcriptionally through the following steps: 1) Methanol induces transcription of genes involved in methanol metabolism leading to the accumulation of methanol-induced mRNAs (mimRNAs) in the cytosol; 2) Multiple mimRNAs accumulate into cytosolic mimRNA granules that contain both ribosome-free and ribosome-associated mimRNAs; 3) mimRNA granules dynamically interact with P-bodies where ribosome-free mimRNAs partially accumulate; 4) In response to environmental stimuli such as oxidative stress, P-bodies actively sequester mimRNAs, protecting them from degradation; 5) Upon stress removal, P-bodies release mimRNAs to the cytosol for translation.

Figure supplements

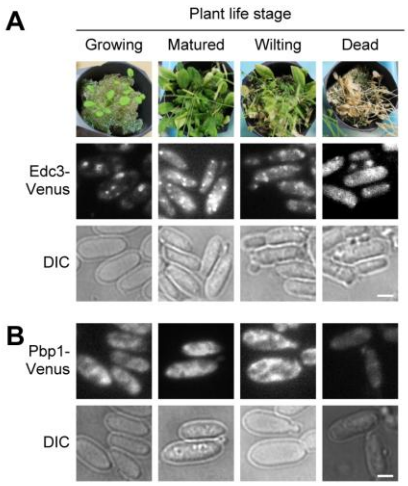

Figure 1–figure supplement 1. Intracellular localization of Edc3-Venus and Pbp1-Venus on *A. thaliana* leaves.

(**A-B**) Investigation of the P-body and SG formation in the WT strains on *Arabidopsis* leaves. Edc3-Venus fusion protein was expressed under the control of the native *EDC3* promoter as a P-body marker (**A**), whereas Pbp1-Venus fusion protein expressed under the control of the native *PBP1* promoter was used as an SG marker (**B**). The strains were spotted on growing, matured, wilting or dead leaves, collected from the leaves 4 hours after inoculation and observed by a fluorescent microscope. Bar, 2 μm. DIC: differential interference contrast.

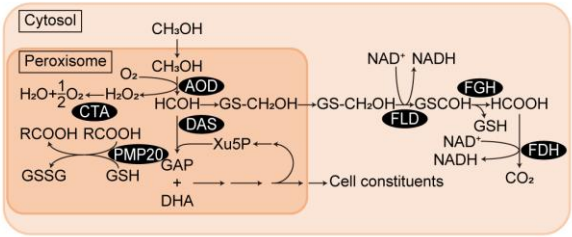

Figure 2–figure supplement 1. Diagram of methanol metabolism in yeast.
Enzymes: AOD, alcohol oxidase; DAS, dihydroxyacetone synthase; FDH, formate dehydrogenase; FGH, *S*-formylglutathione hydrolase; FLD, formaldehyde dehydrogenase; CTA, catalase; PMP20, peroxisome membrane protein with glutathione peroxidase activity. Abbreviations: DHA, dihydroxyacetone; GAP, glyceraldehyde 3-phosphate; GS-CH2OH, S-hydroxymethyl glutathione; GS-CHO, S-formylglutathione; GSH, reduced form of glutathione; GSSG, oxidized form of glutathione; RCOOOH, alkyl hydroperoxide.

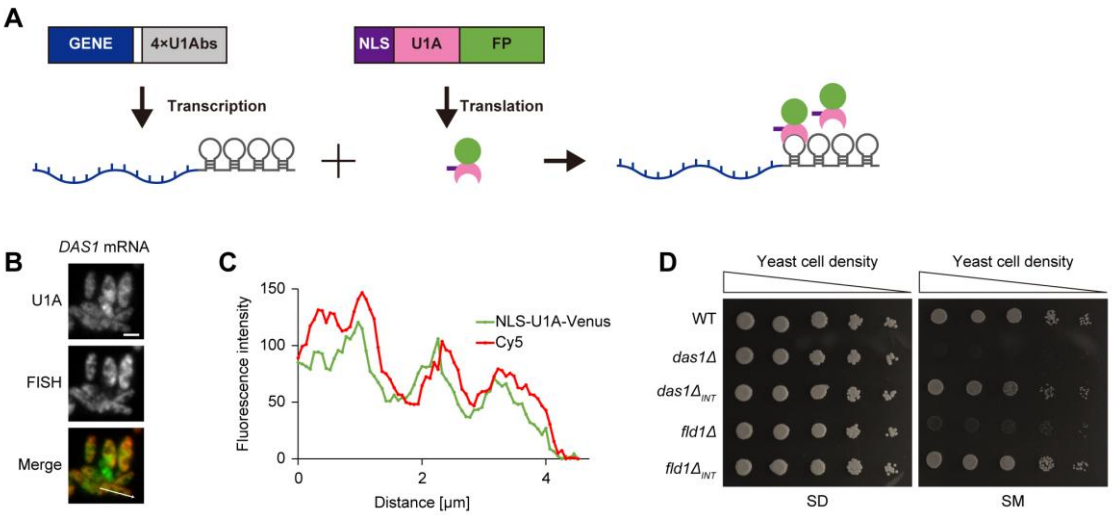

Figure 2–figure supplement 2. Integration of the U1Abs did not alter protein function.

(**A**) Schematic overview for visualizing methanol-induced mRNAs (mimRNAs) *in vivo*. GENE, DNA sequence encoding a target mRNA; White box, UTR; 4xU1Abs, 4 x U1A binding sequence; NLS, nuclear localization sequence; U1A, U1A coding sequence; FP, fluorescent protein coding sequence. Yeast cells were transformed with vectors expressing a fusion of U1Abs with a gene sequence encoding the target mRNA sequence (GENE-4xU1Abs) and a fluorescent protein combined with NLS-U1A (NLS-U1A-FP). GENE-4xU1Abs was expressed under its own promoter, whereas NLS-U1A-FP was expressed under the *TDH3* promoter.

(**B**) Fluorescent microscopic images of *DAS1* mRNA visualized by the U1A-based RNA system and fluorescence *in situ* hybridization (FISH) method. FISH was performed for visualizing the canonical *DAS1* gene (methodological details are described in Materials and Methods section). Strain DAS1m-V grown on an SD medium was transferred to an SM medium and incubated for 3 hours. Merged images were generated by combining Venus and cy5 fluorescence images. Bar: 2 μm.

(**C**) Colocalization of the *DAS1* mRNA detected by the U1A-based RNA system and FISH method in (**B**). mRNA localization was visualized by FISH using Cy5-labeled probes and by the U1A-based RNA system using Venus fluorescence. Fluorescence intensity was measured along a defined line across the cells. Fluorescence intensity (Y-axis) was plotted against distance (X-axis) to show the spatial distribution of mRNA signals.

(**D**) Growth assay of *C. boidinii* strains on SD or SM agar plates. The yeast strains were grown to early log phase, adjusted to OD_{610}=1, and 3μL of tenfold serial dilutions were streaked onto SD or SM plates. The *das1Δ*$_{INT}$ strain expresses 4xU1Abs-tagged native

DAS1 gene under its native promoter and the *fld1Δ*$_{INT}$ strain expresses 4xU1Abs-tagged native *FLD1* gene under its native promoter.

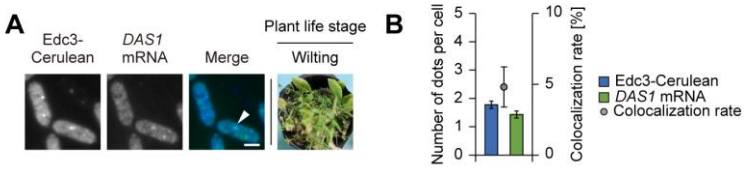

Figure 2–figure supplement 3. Intracellular dynamics of P-bodies and mimRNAs on wilting *A. thaliana* leaves.

(**A**) Fluorescence microscopy images of strain Edc3-C/DAS1m-V on wilting *Arabidopsis* leaves. The strain, spotted on leaves, was collected from the leaf surface 4 hours after inoculation for observation. Merged images were generated by combining Venus and Cerulean fluorescence images. White arrows indicate colocalization of Edc3-Cerulean and Venus-tagged *DAS1* mRNA dots. Bar, 2 µm.

(**B**) Quantification of dot formation of Edc3-Venus and Venus-tagged *DAS1* mRNA and their colocalization detected in (**A**). Cell count analysis was performed on fluorescence microscopy images (n = 30, n: number of cells analyzed; b = 3, b: biological replicates; total = 90 cells). The number of dots is presented as mean ± SE of 90 cells and colocalization rates are shown as mean ± SE from three biological replicates (n = 30 cells per replicate).

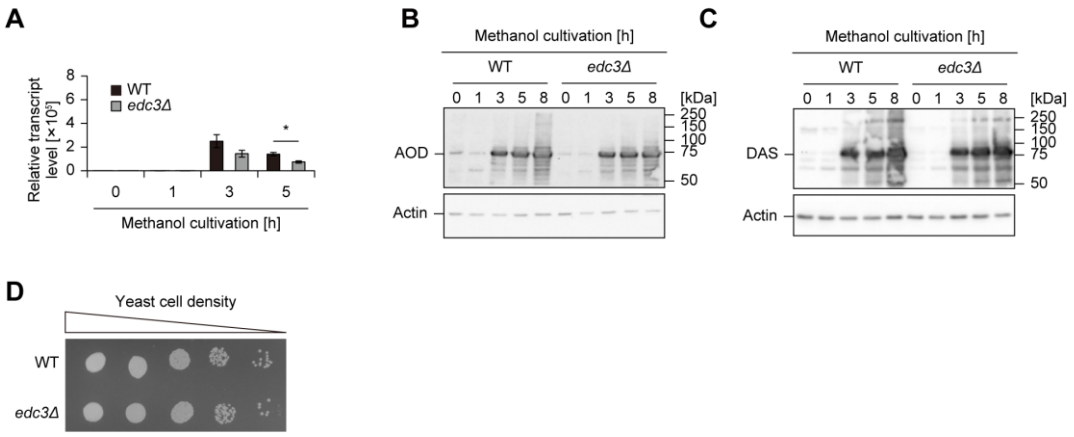

Figure 3–figure supplement 1. Effect of the *EDC3* gene deletion on methanol metabolism.

(**A**) Relative transcript level of *AOD1* mRNA in the WT and *edc3Δ* strains on SM medium. Values are indicated as mean ± SE of three biological replicates. Statistical significances between the WT and *edc3Δ* strains were assessed. Asterisks indicate statistical significance: * $p < 0.05$.

(**B-C**) Immunoblot analysis of AOD (**B**) and DAS (**C**) in the WT and *edc3Δ* strains during methanol induction. The expected molecular weights of AOD and DAS are 74.1 kDa and 78.2 kDa, respectively.

(**D**) Growth assay of cells cultured on methanol. Cells were grown to early log phase, adjusted to OD_{610}=1, and 3 μL of tenfold serial dilutions were dropped onto SM plates. Subsequently, the SM plates were incubated at 28°C. Cell growth was analyzed after 2 days. Growth of the wild-type (WT) and *edc3Δ* was compared.

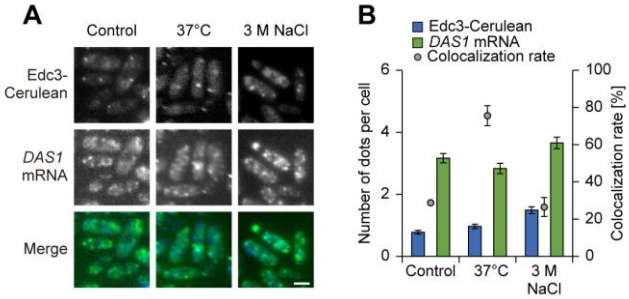

Figure 3–figure supplement 2. Intracellular dynamics of P-bodies and *DAS1* mRNA under stress conditions.

(**A**) Fluorescence microscope images of strain Edc3-C/DAS1m-V during heat and salt stress. The strain was exposed to heat shock at 37 degrees or salt stress with 3 M NaCl for 1 hour before microscopic observation. Merged images were generated by combining Venus and Cerulean fluorescence images. Bar, 2 µm.

(**B**) Quantification of dot formation of Edc3-Venus and Venus-tagged *DAS1* mRNA and their colocalization detected in (**A**). Cell count analysis was performed on fluorescence microscopy images (n = 30, n: number of cells analyzed; b = 3, b: biological replicates; total = 90 cells). The number of dots is presented as mean ± SE of 90 cells and colocalization rates are shown as mean ± SE from three biological replicates (n = 30 cells per replicate).

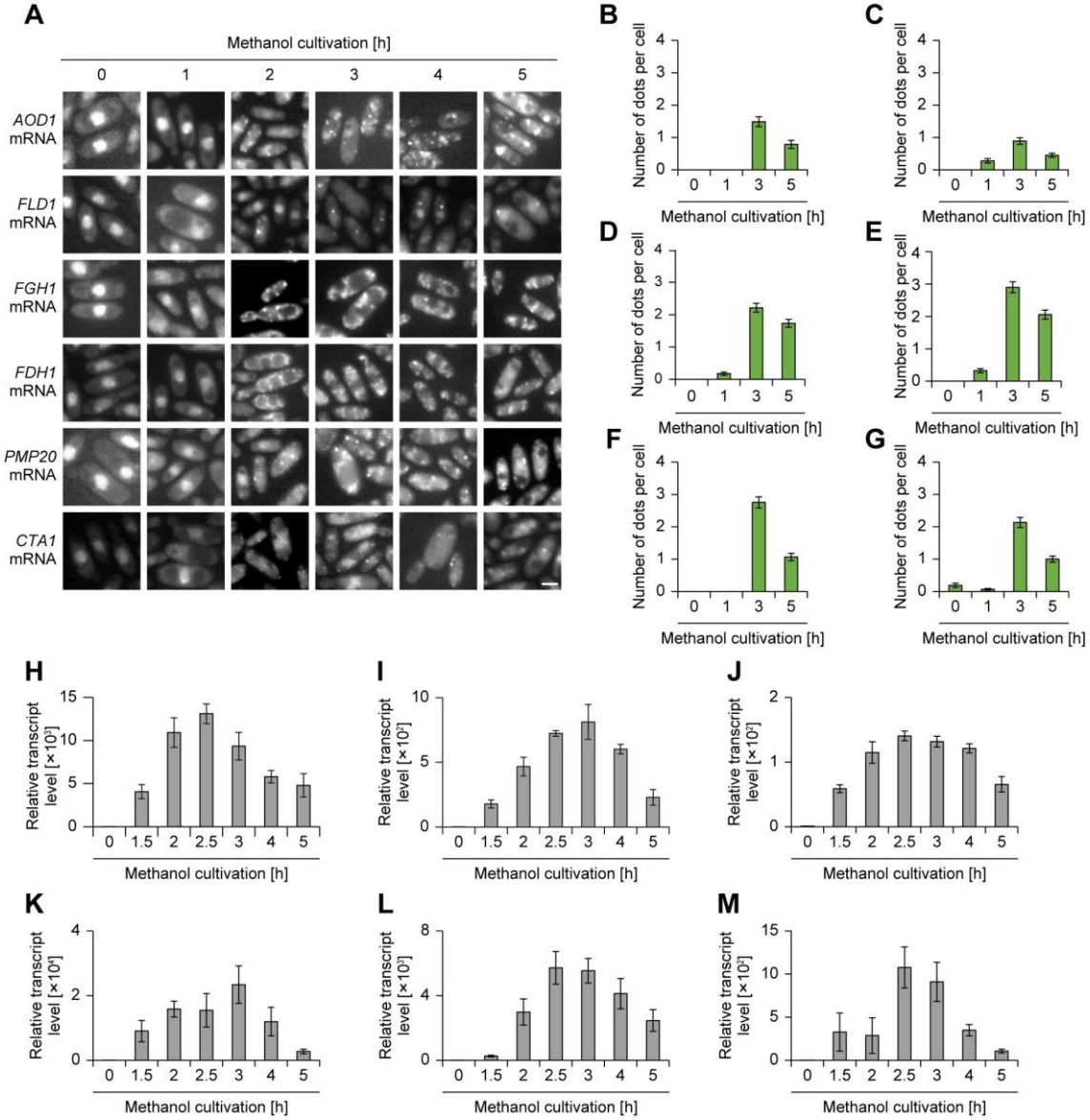

Figure 4–figure supplement 1. Granule formation and gene expression of various mimRNAs during methanol induction.

(**A**) Time-course analysis of the intracellular localization of mimRNAs during methanol induction. *AOD1*, *FLD1*, *FGH1*, *FDH1*, *PMP20* and *CTA1* mRNA were visualized. The strains grown on an SD medium were transferred to SM medium and incubated for up to 5 hours and collected at indicated time points. Bar, 2 µm.

(**B-G**) Quantification of dot formation of mimRNAs detected in (**A**). (**B**) *AOD1*, (**C**) *FLD1*, (**D**) *FGH1*, (**E**) *FDH1*, (**F**) *PMP20* and (**G**) *CTA1* mRNA. At least 30 cells were analyzed per experiment. Cell count analysis was performed on fluorescence microscopy images (n = 30, n: number of cells analyzed; b = 3, b: biological replicates; total = 90

cells). The number of dots is presented as the mean ± SE of 90 cells.

(**H-M**) Relative transcript level of mimRNAs in the WT strain during methanol induction. (**H**) *AOD1*, (**I**) *FLD1*, (**J**) *FGH1*, (**K**) *FDH1*, (**L**) *PMP20* and (**M**) *CTA1* mRNA. Values are indicated as mean ± SE of three independent experiments.

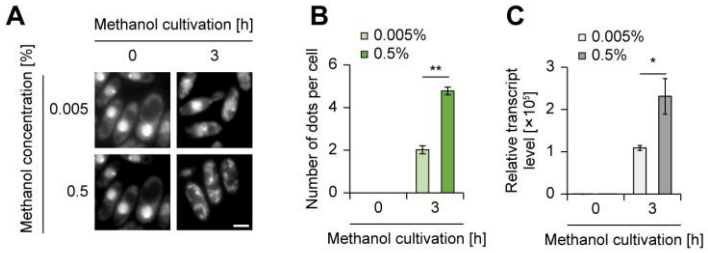

Figure 4–figure supplement 2. Regulation of mimRNA granule formation at low methanol concentration.

(**A**) Fluorescence microscopy images of the strain visualizing Venus-tagged *DAS1* mRNA on SM medium. The strain grown on an SD medium was transferred to SM medium and incubated for 3 hours and collected at indicated time points. Methanol concentration was either 0.0005% or 0.5%. Bar, 2 μm.

(**B**) Quantification of mimRNA granule formation detected in (**A**). Cell count analysis was performed on fluorescence microscopy images (n = 30, n: number of cells analyzed; b = 3, b: biological replicates; total = 90 cells). The number of dots is presented as mean ± SE of of 90 cells. Asterisks indicate statistical significance: ** $p < 0.01$.

(**C**) Relative transcript level of *DAS1* mRNA in the WT strain during methanol induction. Methanol concentration was either 0.0005% or 0.5%. Values are indicated as mean ± SE of three biological replicates. Asterisks indicate statistical significance: * $p < 0.05$.

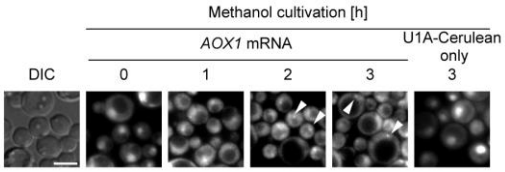

Figure 4–figure supplement 3. Visualization of methanol-induced *KpAOX1* mRNA in *K. phaffii*.

Fluorescent microscopic images of the *K. phaffii* strain expressing U1Abs-tagged *KpAOX1* mRNA, and the NLS- and Cerulean-tagged U1A protein. U1Abs; U1A protein binding sequence, NLS; nuclear localization sequence. The *K. phaffii* strain expressing only U1A-Cerulean (referred to as U1A-Cerulean only) was used as a control in which the Cerulean fluorescence remained in the nucleus. White arrows indicate the dots of *KpAOX1* mRNA. Bar, 2 μm. DIC: differential interference contrast.

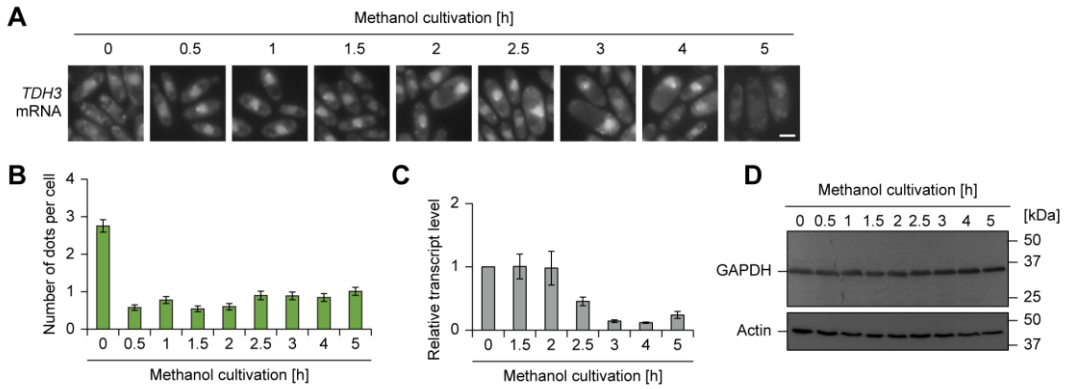

Figure 4–figure supplement 4. Regulation of dot formation of *TDH3* mRNA.

(**A**) Time-course analysis of the intracellular localization of Venus-tagged *TDH3* mRNA during methanol induction. The strain grown on an SD medium was transferred to SM medium and incubated for up to 5 hours. Bar, 2 µm.

(**B**) Quantification of dot formation of Venus-tagged *TDH3* mRNA detected in (**A**). Cell count analysis was performed on fluorescence microscopy images (n = 30, n: number of cells analyzed; b = 3, b: biological replicates; total = 90 cells). The number of dots is presented as mean ± SE of 90 cells.

(**C**) Relative transcript level of *TDH3* mRNA in the WT strain during methanol induction. Values are indicated as mean ± SE of three biological replicates.

(**D**) Immunoblot analysis of GAPDH in the WT strain during methanol induction. The expected molecular weight of GAPDH is 35.5 kDa.

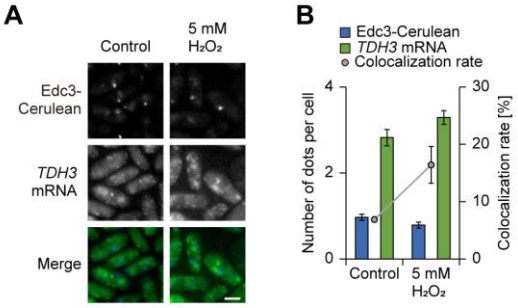

Figure 4–figure supplement 5. Intracellular dynamics of P-bodies and *TDH3* mRNA under stress conditions.

(**A**) Fluorescence microscopy images of strain Edc3-C/TDH3m-V during oxidative stress. The strain incubated on an SM medium was treated with 5 mM H_2O_2 for 1 hour before microscopic observation. Merged images were generated by combining Venus and Cerulean fluorescence images. Bar, 2 µm.

(**B**) Quantification of dot formation of Edc3-Venus and Venus-tagged *TDH3* mRNA and their colocalization detected in (**A**). Cell count analysis was performed on fluorescence microscopy images (n = 30, n: number of cells analyzed; b = 3, b: biological replicates; total = 90 cells). The number of dots is presented as mean ± SE of 90 cells and colocalization rates are shown as mean ± SE from three biological replicates (n = 30 cells per replicate).

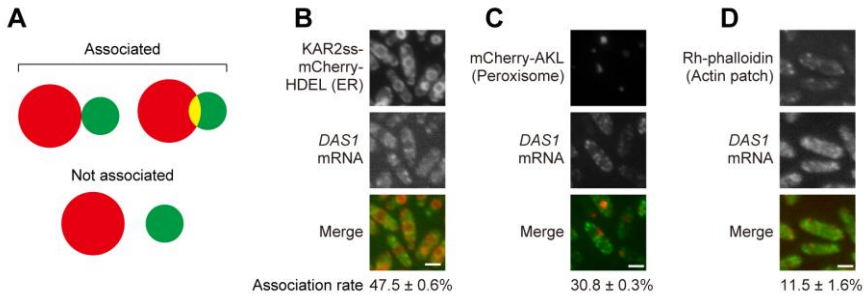

Figure 5–figure supplement 1. Association of mimRNA granules with other organelles and structures.

(**A**) Schematic image of the association or non-association of *DAS1* mRNA with cellular organelles.

(**B-D**) Association of *DAS1* mRNA granules with the endoplasmic reticulum (ER) (**B**), peroxisomes (**C**) and actin patches (**D**). ER was visualized by mCherry tagged with KAR2 sequence signal at its N terminus and HDEL amino acid sequence at its C terminus. Peroxisomes were visualized by mCherry tagged with AKL amino acid sequence at its C terminus for peroxisome targeting signal. Actin patches were stained with rhodamine phalloidin. Cells grown on an SD medium were transferred to an SM medium and incubated for 3 hours. The association rate indicates the percentage of Venus-tagged *DAS1* mRNA granules that are associated with the ER (**B**), peroxisomes (**C**) or actin patches (**D**). Cell count analysis was performed on fluorescence microscopy images (n = 30, n: number of cells analyzed; b = 3, b: biological replicates; total = 90 cells). Association rates are shown as mean ± SE from three biological replicates (n = 30 cells per replicate). Bar, 2 μm.

Legends to videos

Dynamic properties of Edc3-Venus and Venus-tagged *DAS1* mRNA dots during growth on methanol.

Time-lapse images of Edc3-Venus and Venus-tagged *DAS1* mRNA dots (see also Figure 5A) were acquired every 28 seconds for 9 minutes 52 seconds by fluorescence microscopy and compiled into a video at 2 frames per second (fps). Bar, 20 µm.